

**NASA  
Technical  
Memorandum**

NASA TM - 100366

**THE CORROSION PROTECTION OF ALUMINUM  
BY VARIOUS ANODIZING TREATMENTS**

By Merlin D. Danford

Materials and Processes Laboratory  
Science and Engineering Directorate

April 1989

(NASA-TM-100366) THE CORROSION PROTECTION  
OF ALUMINUM BY VARIOUS ANODIZING TREATMENTS  
(NASA. Marshall Space Flight Center) 48 p

CSCL 11F

N89-260 79

G3/26    Unclass    0219844



National Aeronautics and  
Space Administration

George C. Marshall Space Flight Center



**TECHNICAL REPORT STANDARD TITLE PAGE**

1. REPORT NO. NASA TM-100366		2. GOVERNMENT ACCESSION NO.		3. RECIPIENT'S CATALOG NO.	
4. TITLE AND SUBTITLE The Corrosion Protection of Aluminum by Various Anodizing Treatments				5. REPORT DATE April 1989	
				6. PERFORMING ORGANIZATION CODE	
7. AUTHOR(S) Merlin D. Danford				8. PERFORMING ORGANIZATION REPORT #	
9. PERFORMING ORGANIZATION NAME AND ADDRESS George C. Marshall Space Flight Center Marshall Space Flight Center, Alabama 35812				10. WORK UNIT NO.	
				11. CONTRACT OR GRANT NO.	
12. SPONSORING AGENCY NAME AND ADDRESS National Aeronautics and Space Administration Washington, D.C. 20546				13. TYPE OF REPORT & PERIOD COVERED Technical Memorandum	
				14. SPONSORING AGENCY CODE	
15. SUPPLEMENTARY NOTES Prepared by Materials and Processes Laboratory, Science and Engineering Directorate.					
16. ABSTRACT  Corrosion protection to 6061-T6 aluminum, afforded by both teflon-impregnated anodized coats (Polylube and Tufram) and hard-anodized coats (water sealed and dichromate sealed), was studied at both pH 5.5 and pH 9.5, with an exposure period of 28 days in 3.5% NaCl solution (25°C) for each specimen. In general, corrosion protection for all specimens was better at pH 9.5 than at pH 5.5. Protection by a Tufram coat proved superior to that afforded by Polylube at each pH, with corrosion protection by the hard-anodized, water-sealed coat at pH 9.5 providing the best protection. Electrochemical work in each case was corroborated by microscopic examination of the coats after exposure. Corrosion protection by Tufram at pH 9.5 was most comparable to that of the hard-anodized samples, although pitting and some cracking of the coat did occur.					
17. KEY WORDS Electrochemical corrosion measurements AC-impedance method Polarization-resistance method Corrosion protection to 6061-T6 aluminum by anodized coatings				18. DISTRIBUTION STATEMENT  Unclassified - Unlimited	
19. SECURITY CLASSIF. (of this report) Unclassified		20. SECURITY CLASSIF. (of this page) Unclassified		21. NO. OF PAGES 49	
				22. PRICE NTIS	

## **ACKNOWLEDGMENTS**

The author wishes to thank Mr. Wendell DeWeese for the metallographic work, Mrs. Gail Horiuchi of Johnson Space Center for supplying the Polylube and Tufram coated specimens, Mr. Barry Moody for hard anodizing some of the specimens, and Mr. Ralph Higgins for many valuable suggestions during this work.

## TABLE OF CONTENTS

	Page
INTRODUCTION .....	1
EQUIVALENT CIRCUITS .....	1
AC DATA ANALYSIS .....	2
EXPERIMENTAL .....	2
RESULTS AND DISCUSSION .....	3
Polylube at pH 9.5 .....	4
Polylube at pH 5.5 .....	4
Tufram at pH 9.5 .....	5
Tufram at pH 5.5 .....	5
Hard-Anodized, Water-Sealed Coat at pH 9.5 .....	6
Hard-Anodized, Water-Sealed Coat at pH 5.5 .....	6
Hard-Anodized, Dichromate-Sealed Coat at pH 9.5 .....	6
Hard-Anodized, Dichromate-Sealed Coat at pH 5.5 .....	7
CONCLUSIONS .....	7
REFERENCES .....	9

## LIST OF ILLUSTRATIONS

Figure	Title	Page
1.	Circuit representing AC-impedance response for anodized aluminum.....	11
2.	Physical description of circuit parameters for anodized aluminum .....	12
3.	AC-impedance response including chemical reactions.....	13
4.	AC-impedance response including Warburg impedance.....	14
5.	Exploded view of the sample holder .....	15
6.	R(s), R(f), and $I_{CORR}$ -time curves for Polylube coat at pH 9.5.....	16
7.	R(p), R(t), and [R(t) + R(f)]-time curves for Polylube coat at pH 9.5.....	17
8.	Warburg coefficient-time curve for Polylube coat at pH 9.5 .....	18
9.	Top view of Polylube sample exposed to 3.5% NaCl solution at pH 9.5 for 28 days.....	19
10.	Cross section of Figure 9 sample showing depth of corrosion pits.....	19
11.	R(s), R(f), and $I_{CORR}$ -time curves for Polylube coat at pH 5.5.....	20
12.	R(p), R(t), and [R(t) + R(f)]-time curves for Polylube coat at pH 5.5.....	21
13.	Warburg coefficient-time curve for Polylube coat at pH 5.5 .....	22
14.	Top view of Polylube sample exposed to 3.5% NaCl solution at pH 5.5 for 28 days.....	23
15.	Cross section of Figure 14 sample showing depth of corrosion pits .....	23
16.	R(s), R(f), and $I_{CORR}$ -time curves for Tufram coat at pH 9.5 .....	24
17.	R(p), R(t), and [R(t) + R(f)]-time curves for Tufram coat at pH 9.5 .....	25
18.	Warburg coefficient-time curve for Tufram coat at pH 9.5 .....	26
19.	Top view of Tufram sample exposed to 3.5% NaCl solution at pH 9.5 for 28 days.....	27
20.	Cross section of Figure 19 sample showing depth of corrosion pits .....	27

## LIST OF ILLUSTRATIONS (Concluded)

Figure	Title	Page
21.	R(s), R(f), and $I_{CORR}$ -time curves for Tufram coat at pH 5.5 .....	28
22.	R(p), R(t), and [R(t) + R(f)]-time curves for Tufram coat at pH 5.5 .....	29
23.	Warburg coefficient-time curve for Tufram coat at pH 5.5 .....	30
24.	Top view of Tufram sample exposed to 3.5% NaCl solution at pH 5.5 for 28 days.....	31
25.	Cross section of Figure 24 sample showing depth of corrosion pits .....	31
26.	R(s), R(f), and $I_{CORR}$ -time curves for hard-anodized, water-sealed coat at pH 9.5 .....	32
27.	R(p), R(t), and Warburg coefficient-time curves for hard-anodized, water-sealed coat at pH 9.5 .....	33
28.	R(s), R(f), and $I_{CORR}$ -time curves for hard-anodized, water-sealed coat at pH 5.5 .....	34
29.	R(p), R(t), and Warburg coefficient-time curves for hard-anodized, water-sealed coat at pH 5.5 .....	35
30.	Top view of hard-anodized sample exposed to 3.5% NaCl solution at pH 5.5 for 28 days.....	36
31.	Cross sections of Figure 30 sample showing depth of corrosion pit .....	36
32.	R(s), R(f), and $I_{CORR}$ -time curves for hard-anodized, dichromate-sealed coat at pH 9.5.....	37
33.	R(p), R(t), and Warburg coefficient-time curves for hard-anodized, dichromate-sealed coat at pH 9.5.....	38
34.	R(s), R(f), and $I_{CORR}$ -time curves for hard-anodized, dichromate-sealed coat at pH 5.5.....	39
35.	R(p) and R(t)-time curves for hard-anodized, dichromate-sealed coat at pH 5.5 .....	40
36.	Top view of hard-anodized, dichromate-sealed sample exposed to 3.5% NaCl solution at pH 5.5 for 28 days .....	41
37.	Cross section of Figure 36 sample showing depth of corrosion pit .....	41

## LIST OF TABLES

Table	Title	Page
1.	Average Values of Corrosion Currents Obtained by Different Methods .....	10
2.	Summary of Corrosion Pit Size Dimensions .....	10



## TECHNICAL MEMORANDUM

# THE CORROSION PROTECTION OF ALUMINUM BY VARIOUS ANODIZING TREATMENTS

## INTRODUCTION

This work was undertaken because of significant corrosion encountered in the Water Spray Boiler (WSB) on OV-104 using either Polylube or Tufram coatings. Both of these are proprietary Teflon-impregnated aluminum-anodized coatings. In the present case, corrosion effects were studied with samples in contact with 3.5% NaCl solutions buffered at pH 5.5 and pH 9.5, the greater concentration of NaCl being used in order to more quickly observe corrosion currents electrochemically. Corrosion rates and corrosion mechanisms were determined electrochemically using both the AC-impedance and the DC-polarization resistance techniques.

For comparison, hard-anodized (Type III, Class 1 of MIL-A-8625) 6061-T6 aluminum samples, the same alloy used for the Polylube- and Tufram-coated samples, were studied. Samples sealed in either boiling de-ionized water or sodium-dichromate solution were studied at pH 9.5 and pH 5.5. Hard-anodized Type III coatings are intended to provide wear and abrasion resistant surfaces with improved corrosion protection due to greater thicknesses and weight than conventional anodic coatings. When sealed in boiling water, amorphous alumina is converted to boehmite ( $\alpha\text{-Al}_2\text{O}_3\cdot\text{H}_2\text{O}$ ) of greater volume; therefore the smaller the pore before sealing, the smaller will be the sealed pore.  $\text{Na}_2\text{Cr}_2\text{O}_7$  is used as a corrosion inhibiting additive.

## EQUIVALENT CIRCUITS

The basis of the AC-impedance method is the modeling of the corrosion cell in terms of an electronic circuit. A suitable equivalent circuit should reasonably reproduce experimental plots obtained from the corrosion cell. These plots included Bode magnitude (log impedance versus log  $\omega$ , where  $\omega = 2\pi \times$  frequency), Bode phase and complex plane or Nyquist plot ( $-Z''$  versus  $Z'$ ). Equivalent circuit models for coated-metal surfaces are complex, requiring several resistor/capacitor combinations. The equivalent circuit in Figure 1 has been used successfully to represent the response of primer-coated 2219-T87 aluminum [1] and 4130 steel with various primer-topcoat combinations [2]. The physical model this circuit represents is shown in Figure 2.

A second equivalent circuit model, which has been used successfully, is shown in Figure 3. This model generally results in an improved least-squares fit to the observed data, when it can be used. The difference between the two models lies in the addition of a capacitor  $C_{CR}$  to account for a chemical reaction at the metal surface. It has been found [2] that the value of this capacitance is directly proportional to the corrosion current. Once this capacitor is properly calibrated, its value can be used as another means to obtain corrosion rates from AC-impedance data. However, since this capacitor contributes to the total impedance mainly at low frequencies, good low-frequency data must be obtained, a condition which is not always realized.

Another equivalent circuit model, from which the effect of diffusion polarization is obtained, is shown in Figure 4. A contribution due to the Warburg impedance is included in the model of Figure 4, with diffusion polarization giving rise to this effect. It is given by:

$$Z_w = \sigma\omega^{-1/2} - j\sigma\omega^{-1/2} \quad (1)$$

The value of  $\sigma$  is obtained from this model, and generally, the higher the value of  $\sigma$ , the less the diffusion of the surrounding medium through the sample coat. If the value of  $\sigma$  exceeds that of the charge-transfer parameter  $R_t$ , the corrosion is diffusion controlled. It has been suggested that  $\sigma$  be obtained from the Bode magnitude plot by locating the region where the slope of the curve is  $-1/2$  and extrapolating to  $\log \omega = 0$ . However, contributions from the many other components of the equivalent circuit also contribute to the total impedance, resulting in a value of  $\sigma$  which is much too large. Like  $C_{CR}$  in the model of Figure 3, this parameter also has its main effect at small frequencies and, in some cases, the value of  $\sigma$  cannot be obtained for similar reasons. Also, the Warburg impedance parameter of Figure 4 cannot be used in the same model as the capacitor in Figure 3 since both of these parameters contribute at low frequencies, resulting in a strong correlation between the two parameters in a least-squares analysis.

## AC DATA ANALYSIS

The goals of analyzing AC-impedance data are threefold: (1) determine the equivalent circuit that most accurately describes the corrosion cell; (2) assign the best possible values to resistors and capacitors in the equivalent circuit for that particular experiment (for this program it was found that experiments should be run every other day for four weeks); and (3) determine the best parameters in the equivalent circuit to fit the observed data. As sample immersion continues, all model parameters change, some more than others.

Reference 1 outlines the method for obtaining starting parameters from experimental Nyquist plots. These values are read into a complex least-squares program, which is based on an adaptation of the general non-linear least-squares program ORGLS [3]. It gives best values for parameters of the equivalent circuit.

## EXPERIMENTAL

Polylube- and Tufam-coated 6061-T6 aluminum samples were supplied by the Johnson Space Center. These samples were in the form of aluminum disks 1.43 cm (0.563 in) in diameter and approximately 0.16 cm (0.063 in.) thick, coated on both sides with 40 microns (1.6 mil) of either the Polylube or Tufam materials. One side of each specimen was then sanded to bare metal for electrical contact when placed in the sample holder shown in Figure 5. Sample surfaces were subsequently wiped with denatured alcohol to remove fingerprints which would otherwise interfere with the experiments. Hard-anodized specimens of the same sample dimensions were prepared

using the alumilite process and sealed using either boiling de-ionized water or a 1 percent  $\text{Na}_2\text{Cr}_2\text{O}_7$  solution. Coating thickness for the water-sealed samples was 25 microns (1.0 mil) and that for the dichromate-sealed samples was 45 microns (1.8 mil). The samples were immersed for 28 days in 3.5% NaCl solutions buffered at pH 5.5 and pH 9.5.

AC-impedance and DC-polarization resistance measurements (where possible) were made on alternate days for the entire test period. The EG&G-PARC Model 378 AC-impedance system was used for the AC-impedance measurements. These data were taken in three sections. The first two sections, beginning at 0.001 Hz and 0.1 Hz respectively, were obtained using the Fast Fourier Transform Technique. The last section, ranging from 5.1 to 80,000 Hz, was collected using the lock-in amplifier technique. The sequencing was performed automatically using the auto-execute procedure, with all data being merged to a single set for each run. The period of collection for the AC-impedance data was approximately 3 hr. After collection, the data were processed and analyzed with the IBM PC/AT computer, which was also used for system control, using the equivalent circuit models of Figures 1, 3, and 4.

Data were collected for the polarization-resistance method using the same system with the EG&G-PARC Model 342 software, which was developed especially for DC measurements. The data were automatically corrected during the scan for IR drop using the technique developed by EG&G-PARC and analyzed using the program POLCURR [4]. The theory for the polarization resistance technique has been described previously [5].

## RESULTS AND DISCUSSION

Throughout this section,  $I_{\text{CORR}}$  will be estimated from AC-impedance data using the relation:

$$I_{\text{CORR}} = \frac{ba \times bc}{2.303(ba + bc)} \cdot \frac{1}{(R_t + R_f)} \quad (2)$$

which is the Stern-Geary equation for charge-transfer control [6-8]. Tafel constants (ba and bc) were estimated to be 50 mV each, and  $(R_t + R_f)$  is the total charge-transfer resistance. Values for  $I_{\text{CORR}}$  thus obtained were eventually compared to those obtained using  $C_{\text{CR}}$  and with polarization resistance measurements where possible. The corrosion in mils/year is obtained through the relation:

$$\text{Corrosion rate (mpy)} = 0.1280 I_{\text{CORR}} (\text{Eq. Wt.})/\rho \quad (3)$$

where

$$I_{\text{CORR}} = \text{corrosion current density, } \mu\text{A/cm}^2$$

Eq. Wt. = equivalent weight of corroding species, gm

$\rho$  = density of corroding species, gm/cm<sup>3</sup> .

For 6061-T6 aluminum, equation (3) becomes:

$$\text{Corrosion rate (mpy)} = 0.42635 \times I_{\text{CORR}} \quad (4)$$

The equation used for obtaining the corrosion current from the value of the capacitor  $C_{\text{CR}}$  [2] is:

$$I_{\text{CORR}} (\mu\text{A/cm}^2) = 3.4074 \times 10^{-5} C_{\text{CR}} (\text{microfarads}) \quad (5)$$

### **Polylube at pH 9.5**

Curves for  $R(s)$ ,  $R(f)$ , and  $I_{\text{CORR}}$  versus time for Polylube at pH 9.5 are shown in Figure 6, with similar curves for  $R(p)$ ,  $R(t)$ , and  $[R(f) + R(t)]$  shown in Figure 7. The curve for variation of sigma, the diffusion parameter, is shown in Figure 8. Corrosion kinetics are charge-transfer controlled, with  $R(t)$  starting at approximately 174 k $\Omega$  at 1 day and  $R(f)$  starting at approximately 11 k $\Omega$ . As the curves indicate, there is general breakdown of corrosion protection after approximately 13 days. However, values of the curves rise thereafter and it appears that corrosion damage is self-healing at this pH. This is probably due to the sealing of corrosion spots by the corrosion products, which might be less soluble at pH 9.5. Trends for the diffusion curve in Figure 8 are the same as those for the resistance curves, while  $I_{\text{CORR}}$  rises to a maximum at 13 days, and thereafter drops to a relatively low value. As stated previously, the  $I_{\text{CORR}}$  curves shown are calculated using equation (2). The sample was examined metallographically at the end of the test period. Examination showed a single pit 580 microns (Fig. 9) in diameter with a depth of 110 microns (Fig. 10). A highly-magnified view of the film cross section showed several cracks extending to the metal surface. The average value of  $I_{\text{CORR}}$  for the run duration was 0.1422  $\mu\text{A/cm}^2$ , as obtained using the assumptions in equation (2).

### **Polylube at pH 5.5**

Curves for  $R(s)$ ,  $R(f)$ , and  $I_{\text{CORR}}$  versus time are shown in Figure 11, and those for  $R(p)$ ,  $R(t)$ , and  $[R(t) + R(f)]$  are shown in Figure 12. A curve for the time variation of the diffusion coefficient is shown in Figure 13. The  $R(t)$  curve at pH 5.5 begins at 16,617 k $\Omega$  and that for  $R(f)$  at 290 k $\Omega$ , much larger values than were observed at pH 9.5. However, these values drop to a rather low level at approximately 10 days.  $I_{\text{CORR}}$  becomes observable at 10 days and continues to rise rather steeply with time. The diffusion parameter curve shows a trend similar to that for the resistance curves, with diffusion becoming prevalent after 10 days. The average value of the corrosion current over the 28-day exposure period was 0.2163  $\mu\text{A/cm}^2$ , the highest value observed for

any of these systems. Microscopic examination of the sample after exposure showed a single pit with a diameter of 740 microns and a depth of 290 microns (Figs. 14 and 15), which was also the largest pit observed in this work. A photograph of the sample cross section taken at high magnification showed the film to be in extremely poor condition, much inferior to that at pH 9.5.

### Tufram at pH 9.5

Curves for  $R(s)$ ,  $R(f)$ , and  $I_{CORR}$  versus time are shown in Figure 16, and those for  $R(p)$ ,  $R(t)$ , and  $[R(t) + R(f)]$  are shown in Figure 17. A curve for the diffusion coefficient versus time is shown in Figure 18. The value of the curve for  $R(t)$  versus time begins at 1,235 k $\Omega$  at 3 days, while that for  $R(f)$  versus time starts at 33 k $\Omega$ . However, the curve for total charge-transfer resistance rises rapidly for approximately 16 days to a value of approximately 120,000 k $\Omega$ , then to a minimum value rather suddenly at 18 days. As with Polylube at pH 9.5, the corrosion damage again appears to be self-healing, with the total charge-transfer resistance curve rising one more after the 18-day minimum. The  $I_{CORR}$  versus time curve shows a maximum at 18 days, falling rapidly to a minimal value thereafter. The diffusion coefficient-time curve shows a trend similar to that for the resistance-time curves. The value of the diffusion coefficient was rather large (52,478 k $\Omega \cdot \text{sec}^{-1/2}$ ) at its maximum value, and was generally much larger than values for Polylube at either pH 5.5 or pH 9.5, as were values for the charge-transfer resistance. The average corrosion current for the 28-day period was only 0.0009  $\mu\text{A}/\text{cm}^2$ , which is much lower than the corresponding value for Polylube. Microscopic examination at the end of the 28-day period (Figs. 19 and 20) revealed a single pit 465 microns in diameter and 110 microns deep. A highly-magnified view of the film cross section showed it to be in fairly good condition. A few cracks were apparent, but none extended from the film surface to the metal. The film condition was, in general, much better than that for Polylube at pH 9.5.

### Tufram at pH 5.5

Curves for  $R(s)$ ,  $R(f)$ , and  $I_{CORR}$  versus time are shown in Figure 21, and those for  $R(p)$ ,  $R(t)$ , and  $[R(t) + R(f)]$  are shown in Figure 22. The diffusion-coefficient time curve is shown in Figure 23. The  $R(t)$ -time curve begins at a value of 122,821 k $\Omega$  at day 2, while the  $R(f)$ -time starts at a value of 3,799 k $\Omega$ . These values are, thus, higher than those for the Tufram sample at pH 9.5, but contrary to the behavior of these curves at pH 9.5 (values of the curve at pH 9.5 become much larger after several days), the  $R(t)$ -time curve at pH 5.5 reaches a minimum at approximately 5 days, increases only slightly, and drops slowly thereafter. Behavior of the  $R(f)$ -time curve is similar, as is that of the diffusion parameter-time curve in Figure 23, with the value of the diffusion parameter generally being much smaller at pH 5.5 than at pH 9.5. In all of these cases, corrosion is indicated to be charge-transfer controlled (values of the total charge-transfer resistance are larger than  $\sigma$ ). The  $I_{CORR}$ -time curve in Figure 21 shows a rather constant value up to 20 days and then rises rapidly, reaching a peak value at approximately 23 days. The average value of  $I_{CORR}$  for the 28-day period was 0.0389  $\mu\text{A}/\text{cm}^2$ , much larger than the value of pH 9.5 (0.0009  $\mu\text{A}/\text{cm}^2$ ). Again, microscopic examination at the end of the exposure time showed a single pit, 465 microns in diameter with a depth of 110 microns (Figs. 24 and 25). A cross section of the film at high magnification showed a few cracks in the film surface. In general, the

condition of the film for the Tufram-coated specimens was superior to that for Polylube-coated specimens, and the electrochemical data curves also indicate superior protection by this coating. Corrosion protection was, in general, better at pH 9.5 than at pH 5.5 for all specimens.

### **Hard-Anodized, Water-Sealed Coat at pH 9.5**

Curves for  $R(s)$ ,  $R(f)$ , and  $I_{CORR}$  versus time are shown in Figure 26, with those for  $R(p)$ ,  $R(t)$ , and the diffusion parameter shown in Figure 27. Values for  $R(t)$  started at 27,381 k $\Omega$  at 1 day, while those for  $R(f)$  started at about 12k $\Omega$ . Values for  $R(t)$  and  $R(f)$  generally increased with time, as was the case for Tufram at the same pH. This is another indication of the corrosion-damage healing effect at pH 9.5. The value of the diffusion parameter also increased and reached a rather constant level after 10 days. The  $I_{CORR}$  versus time curve showed a slowly decreasing trend, consistent with the trends observed for the resistance-time and diffusion parameter-time curves. Values of  $R(t)$  and  $R(f)$  are generally about the same as the values observed for Tufram at the same pH, as well as are the values for the diffusion parameter. However, the average value of  $I_{CORR}$  over the 28-day period was only 0.00014  $\mu A/cm^2$ , slightly less than that for Tufram (0.0009  $\mu A/cm^2$ ). Microscopic examination of the sample surface after the 28-day immersion showed no indication of any pits, while a magnified view of the film cross section showed it to be in excellent condition, with no apparent cracking.

### **Hard-Anodized, Water-Sealed Coat at pH 5.5**

$R(s)$ ,  $R(f)$ , and  $I_{CORR}$ -time curves are shown in Figure 28, and those for  $R(p)$ ,  $R(t)$ , and the diffusion parameter are shown in Figure 29. Values of  $R(t)$  start at 11,389 k $\Omega$  at 2 days, while  $R(f)$  starts at approximately 10 k $\Omega$ . The value of  $R(t)$ , the dominating factor in the charge-transfer process, increases gradually, and drops to a minimum at 18 days, rising to a peak maximum of about 5,600 k $\Omega$  thereafter. The diffusion parameter curve in Figure 29 shows similar trends. Values of  $R(t)$  are generally an order of magnitude lower than those for the hard-anodized, water-sealed coat at pH 9.5, as are the values of the diffusion parameter. Microscopic examination of the sample surface at the end of the 28-day period showed a single pit 700 microns in diameter and 176 microns deep (Figs. 30 and 31). A highly-magnified view of the film cross section showed the film to be in excellent condition otherwise, with no visible cracking, as was the case for the Tufram and Polylube samples. The average corrosion current for the 28-day test period was 0.0130  $\mu A/cm^2$ .

### **Hard-Anodized, Dichromate-Sealed Coat at pH 9.5**

Curves for  $R(s)$ ,  $R(f)$ , and  $I_{CORR}$  versus time are shown in Figure 32, with those for  $R(p)$ ,  $R(t)$  and the diffusion parameter shown in Figure 33. Values of  $R(t)$  started at 11,000 k $\Omega$  at 2 days, while those for  $R(f)$  started at 2.4 k $\Omega$ . Values of  $R(t)$  and  $R(f)$  are notably less than those obtained for the hard-anodized, water-sealed coat at the same pH. The diffusion coefficient shows similar behavior. This effect is attributed to the ionic nature of the dichromate sealant. The  $R(t)$ -time curve reached a minimum value after about 19 days without continuing to decrease, while the  $R(f)$ -time curve increased with time. According to these results, the corrosion process is again

charge-transfer controlled. The corrosion rate showed a rather sudden increase at approximately 16 days, reaching a maximum at 19 days and thereafter slowly decreasing. The average value of the corrosion current in this case was  $0.0075 \mu\text{A}/\text{cm}^2$ . This is to be compared to a value of  $0.00014 \mu\text{A}/\text{cm}^2$  for the water-sealed coat at pH 9.5. Apparently, the smaller pore size resulting from the water sealing is more effective than the corrosion inhibitive nature of the dichromate ion, and the higher value of the corrosion current in the hard-anodized, dichromate-sealed coat is a reflection of the lower charge-transfer resistance caused by the ionic species ( $\text{Cr}_2\text{O}_7^-$ ) present. Microscopic examination after the 28-day immersion in 3.5% NaCl solution showed no pits, as was also the case for the hard-anodized, water-sealed coat. A highly magnified view of the film cross section again showed it to be in excellent condition, with no cracking visible.

### Hard-Anodized, Dichromate-Sealed Coat at pH 5.5

Curves for  $R(s)$ ,  $R(f)$ , and  $I_{\text{CORR}}$  versus time are shown in Figure 34, with those for  $R(p)$  and  $R(t)$  shown in Figure 35. The diffusion parameter-time curve is not shown in this case because the number of points obtained experimentally was not sufficient. Values of the  $R(t)$ -time and  $R(f)$ -time curves are much the same as those for the hard-anodized, dichromate-sealed coat at pH 9.5, and exhibited the same trends. The  $I_{\text{CORR}}$ -time curve displayed an oscillating nature, with values of the diffusion parameter which were obtained correlating well with positions of the maxima and minima. The average value of the corrosion current in this case was  $0.0136 \mu\text{A}/\text{cm}^2$ , approximately the same as that for the hard-anodized, water-sealed coat at pH 5.5. As with all samples, corrosion effects are less at pH 9.5 than at pH 5.5. However, microscopic examination of the sample after the 28-day exposure to a 3.5% NaCl solution revealed a small pit at this pH, 145 microns in diameter and 145 microns deep (Figs. 36 and 37). This pit is, thus, much smaller than that obtained in the hard-anodized, water-sealed specimen at the same pH, although this may be partially due to the thicker coat on this sample. A cross section at high magnification again showed the coat to be in otherwise relatively good condition.

## CONCLUSIONS

All coatings in this work have been exposed to an environment (3.5% NaCl solution) much more corrosive than that encountered in practice, and corrosion rates are much accelerated. However, as a general rule, corrosion rates are doubled or trebled for each 10 deg of temperature elevation. Therefore, the corrosion rates may be somewhat compensatory, since all samples in this work were exposed at 25 °C.

Average values of corrosion currents by different methods are summarized in Table 1. In general, corrosion currents obtained by AC-impedance methods are in good agreement with those obtained with the DC-polarization resistance method. All corrosion reactions are charge-transfer controlled, and, generally, curves obtained with the AC-impedance method (both magnitudes and trends) are corroborated by microscopic examination of the specimens after exposure. Pitting was found for all specimens except those for the hard-anodized coats at pH 9.5 for both the water-sealed and dichromate-sealed specimens, although the pit at pH 5.5 for the hard-anodized,

dichromate-sealed coat was very small. The pit sizes observed are summarized in Table 2. Corrosion in all cases was more pronounced at pH 5.5 than at pH 9.5. There seemed to be a tendency toward a healing effect at pH 9.5, probably caused by a less soluble nature of corrosion products at this pH.

Tufram, in general, exhibited better corrosion protection than Polylube, both at pH 9.5 and pH 5.5. Greatest deterioration of the coat occurred with Polylube at pH 5.5. However, some cracking occurred in all Teflon-impregnated anodized coatings at both pH 5.5 and pH 9.5. The best corrosion protection was afforded by a hard-anodized, water-sealed coat at pH 9.5. No pitting was encountered with this sample, and microscopic examination showed the coat to be in excellent condition after exposure. Similar behavior was encountered for the hard-anodized, dichromate-sealed coat at pH 9.5, although the corrosion current was somewhat higher. Although some pitting occurred at pH 5.5 for both of these specimens, the coating condition was otherwise good for both. As a result of this study, it is recommended that the use of hard anodizing in the water-spray boilers of the Orbiter be considered, with the water contained therein maintained at a pH of approximately 9.5.



## REFERENCES

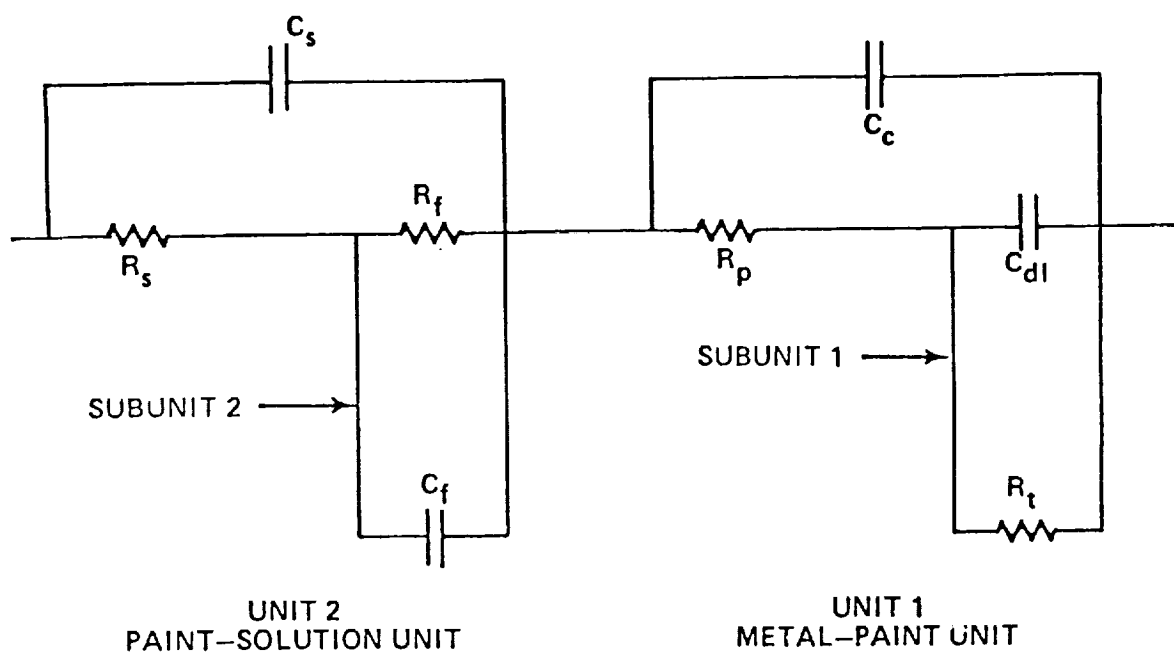
1. Danford, M.D. and Knockemus, M.W.: The Corrosion Mechanisms for Primer Coated 2219-T87 Aluminum. NASA Technical Paper 2715, April 1987.
2. Mendrek, M.J., Higgins, R.H., and Danford, M.D.: An Electrochemical Study of Corrosion Protection by Primer-Topcoat Systems on 4130 Steel with AC Impedance and DC Methods. NASA Technical Paper 2820, May 1988.
3. Busing, W.R. and Levy, H.A.: A General Non-Linear Least Squares Program, ORGLS. Oak Ridge National Laboratory, 1958.
4. Gerchakov, S.M., Udey, L.R., and Mansfeld, F.: An Improved Method for Analysis of the Polarization Resistance Data. Corrosion, Vol. 37, 1981, p. 696.
5. Danford, M.D. and Higgins, R.H.: An Electrochemical Study of the Corrosion of Primer Coated 2219-T87 Aluminum. NASA Technical Paper 2459, April 1985.
6. Stern, M. and Geary, A.L.: Journal of the Electrochemical Society, Vol. 102, 1955, p. 609.
7. Stern, M. and Geary, A.L.: Journal of the Electrochemical Society, Vol. 104, 1957, p. 56.
8. Stern, M.: Corrosion, Vol. 14, 1958, p. 440t.

TABLE 1. AVERAGE VALUES OF CORROSION CURRENTS OBTAINED BY DIFFERENT METHODS

Material	pH	From Equation (2), $\mu\text{A}/\text{cm}^2$	From $C_{\text{CR}}$ $\mu\text{A}/\text{cm}^2$	From Pol. Res., $\mu\text{A}/\text{cm}^2$
Polylube	9.5	0.1422	0.0427	0.0769
	5.5	0.2163	0.1024	0.2117
Tufram	9.5	0.0009	0.0003	—
	5.5	0.0389	0.0180	0.0341
Hard-Anodized Water-Sealed	9.5	0.0001	0.0001	—
	5.5	0.0130	0.0094	0.0183
Hard-Anodized $\text{Na}_2\text{Cr}_2\text{O}_7$ Sealed	9.5	0.0075	0.0078	0.0117
	5.5	0.0136	0.0234	0.0199

TABLE 2. SUMMARY OF CORROSION PIT SIZE DIMENSIONS

Material	pH	Pit Diameter, Microns	Pit Depth Microns
Polylube	9.5	580	110
	5.5	740	290
Tufram	9.5	465	110
	5.5	560	130
Hard-Anodized Water-Sealed	9.5	—	—
	5.5	700	176
Hard-Anodized $\text{Na}_2\text{Cr}_2\text{O}_7$ Sealed	9.5	—	—
	5.5	145	145



$C_s$	SOLUTION CAPACITANCE
$R_s$	SOLUTION RESISTANCE
$C_f$	FARADAIC CAPACITANCE (COATING/SOLUTION)
$R_f$	FARADAIC RESISTANCE
$C_c$	COATING CAPACITANCE
$R_p$	COATING RESISTANCE
$C_{dl}$	METAL/COATING INTERFACE CAPACITANCE
$R_t$	CHARGE TRANSFER RESISTANCE

Figure 1. Circuit representing AC-impedance response for anodized aluminum.

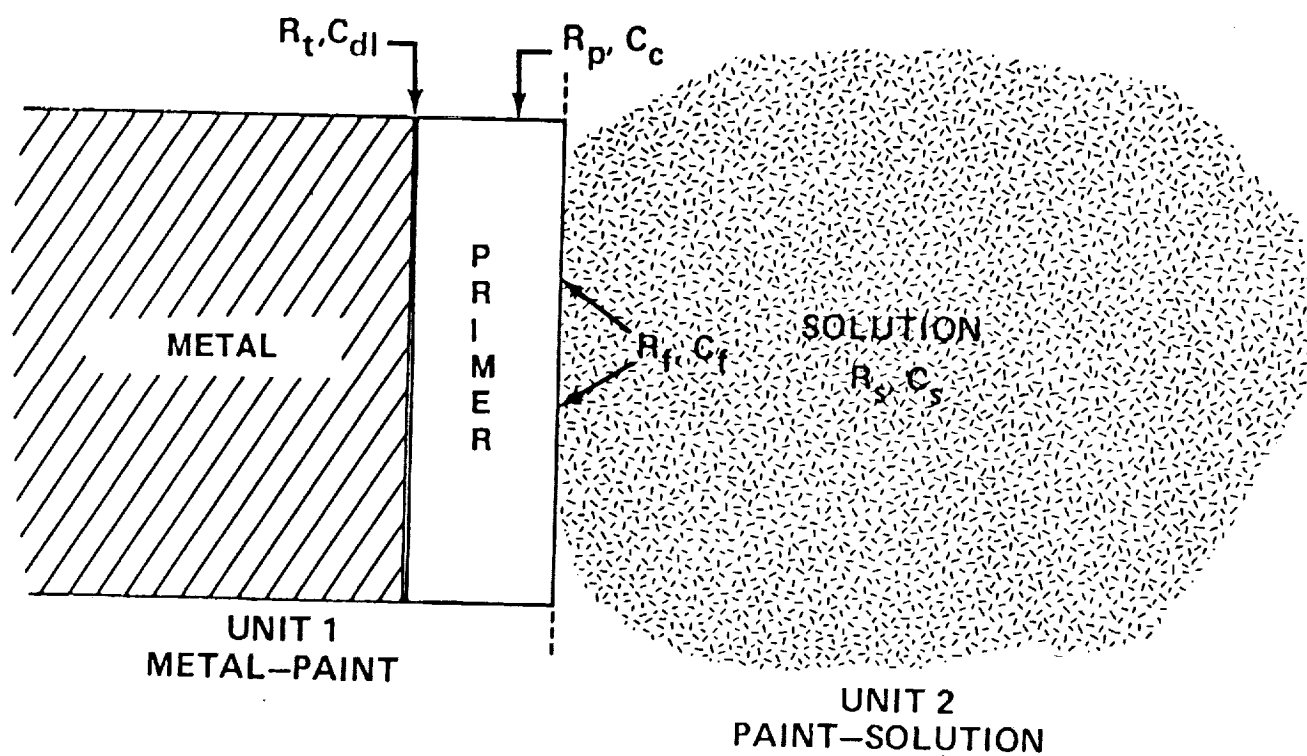
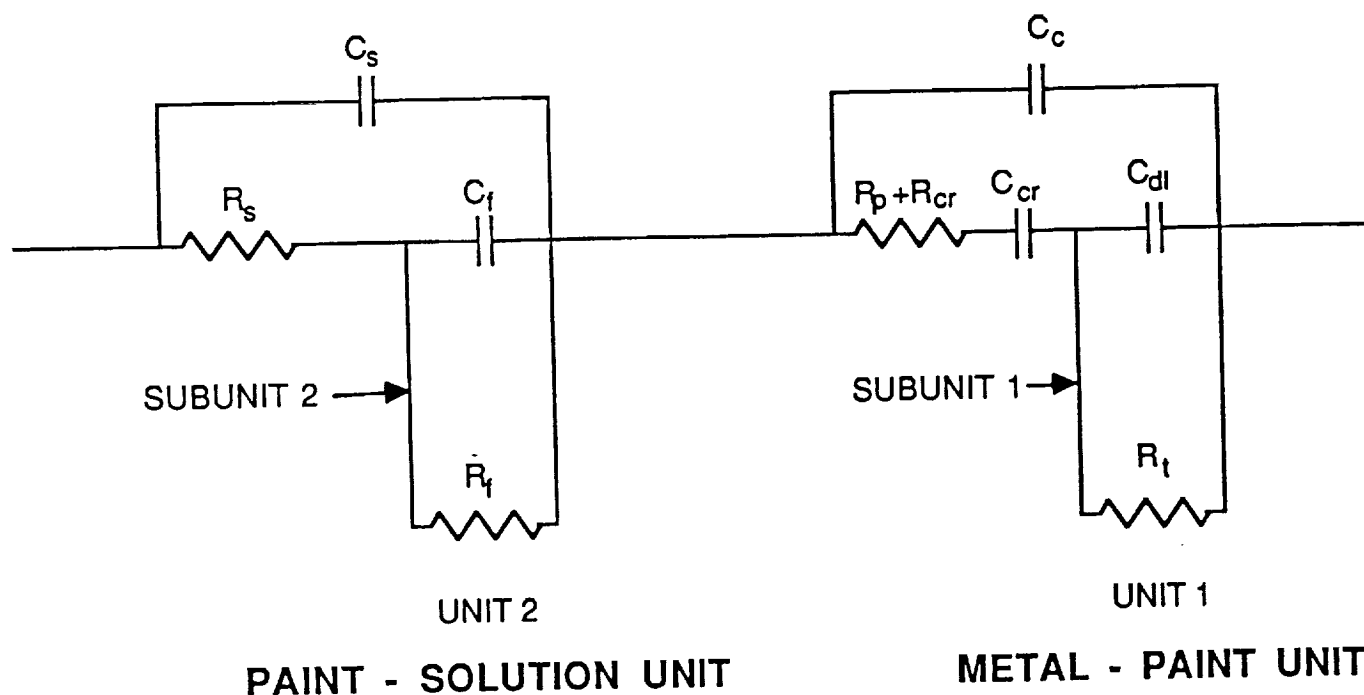
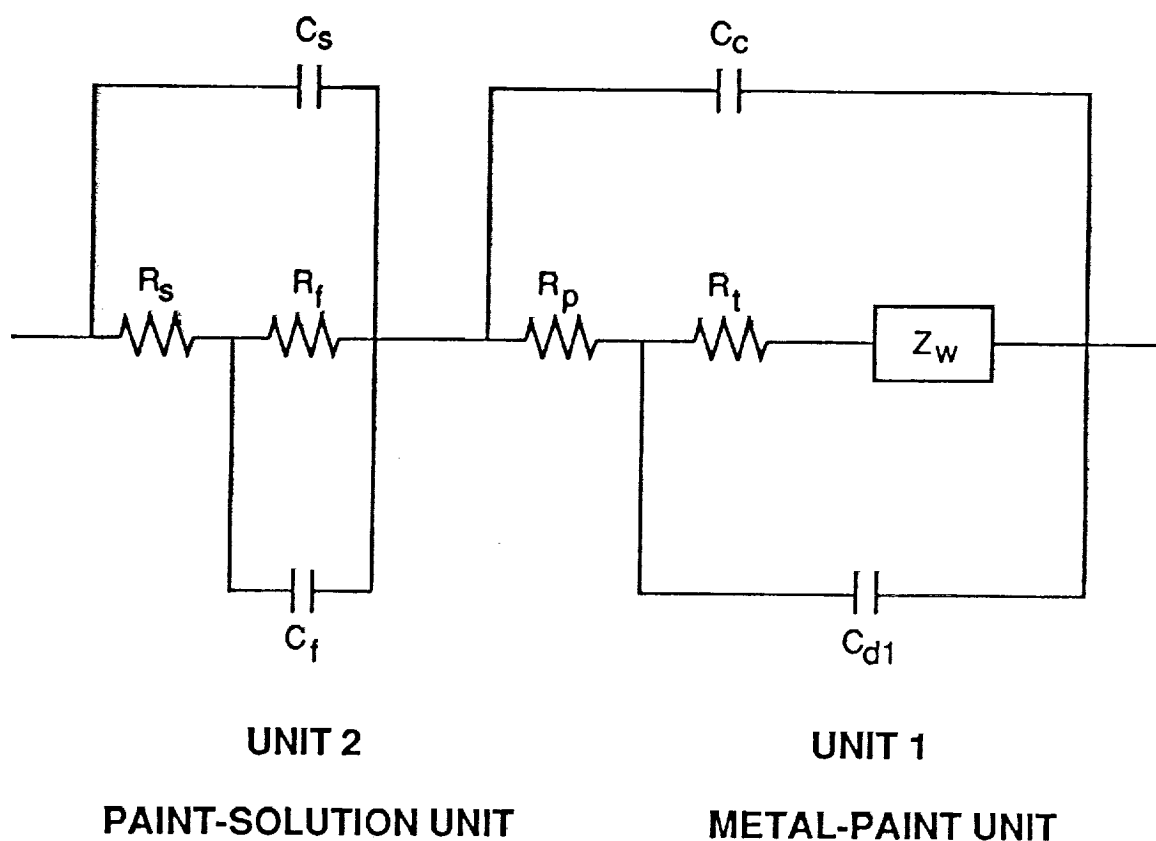


Figure 2. Physical description of circuit parameters for anodized aluminum.



$C_s$	SOLUTION CAPACITANCE
$R_s$	SOLUTION RESISTANCE
$C_f$	FARADAIC CAPACITANCE (COATING/SOLUTION)
$R_f$	FARADAIC RESISTANCE
$C_c$	COATING CAPACITANCE
$R_p + R_{cr}$	COATING RESISTANCE + CHEMICAL REACTION RESISTANCE
$C_{dl}$	METAL/COATING INTERFACE CAPACITANCE
$R_t$	CHARGE TRANSFER RESISTANCE
$C_{cr}$	CHEMICAL REACTION CAPACITANCE

Figure 3. AC-impedance response including chemical reactions.



- $C_s$  SOLUTION CAPACITANCE
- $R_s$  SOLUTION RESISTANCE
- $C_f$  FARADAIC CAPACITANCE (COATING/SOLUTION)
- $R_f$  FARADAIC RESISTANCE
- $C_c$  COATING CAPACITANCE
- $R_p$  COATING RESISTANCE
- $R_t$  CHARGE TRANSFER RESISTANCE
- $C_{d1}$  METAL/COATING INTERFACE CAPACITANCE
- $Z_w$  WARBURG IMPEDENCE (DIFFUSION POLARIZATION)

Figure 4. AC-impedance response including Warburg impedance.

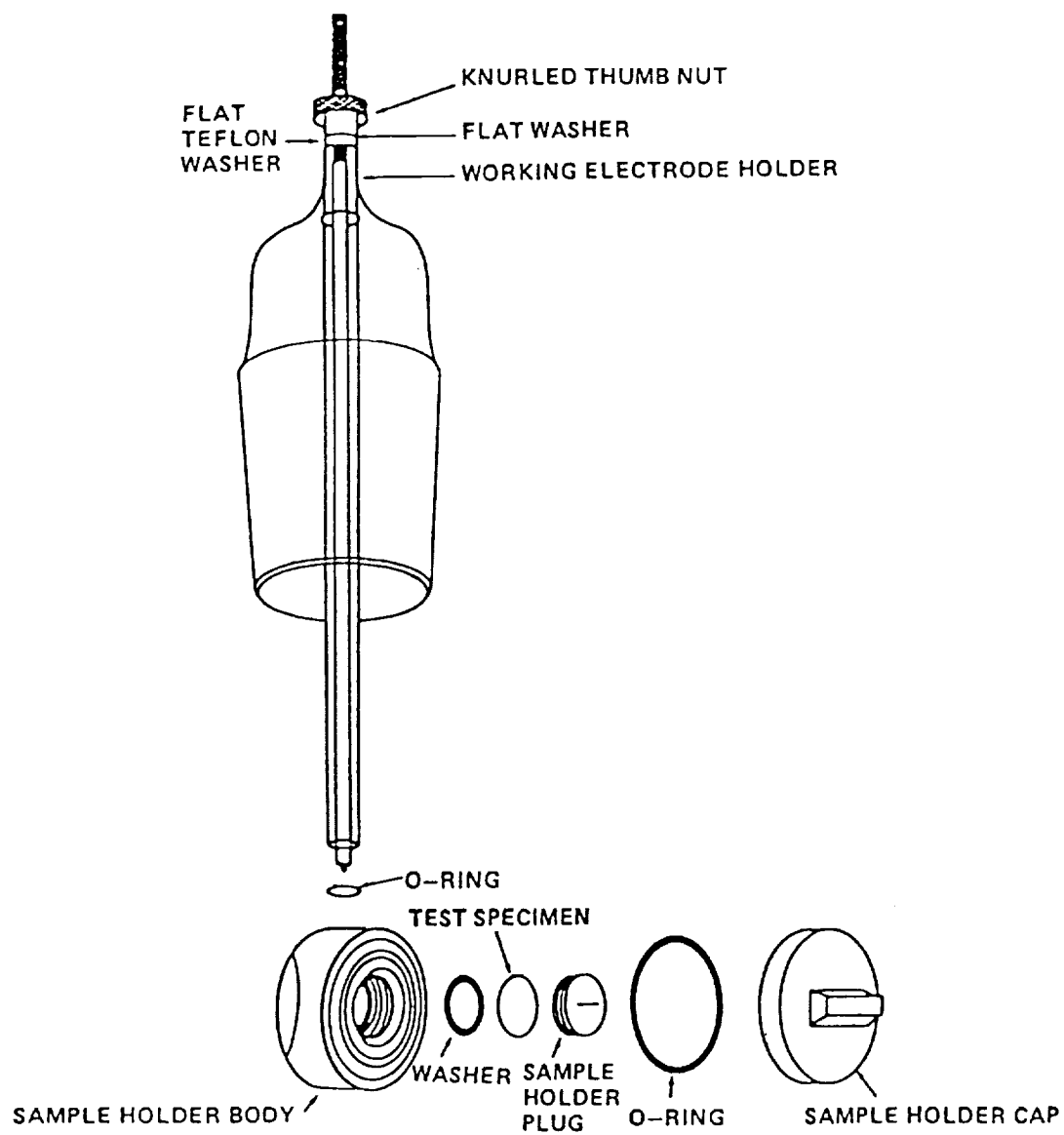


Figure 5. Exploded view of the sample holder.

## POLYLUBE, pH 9.5

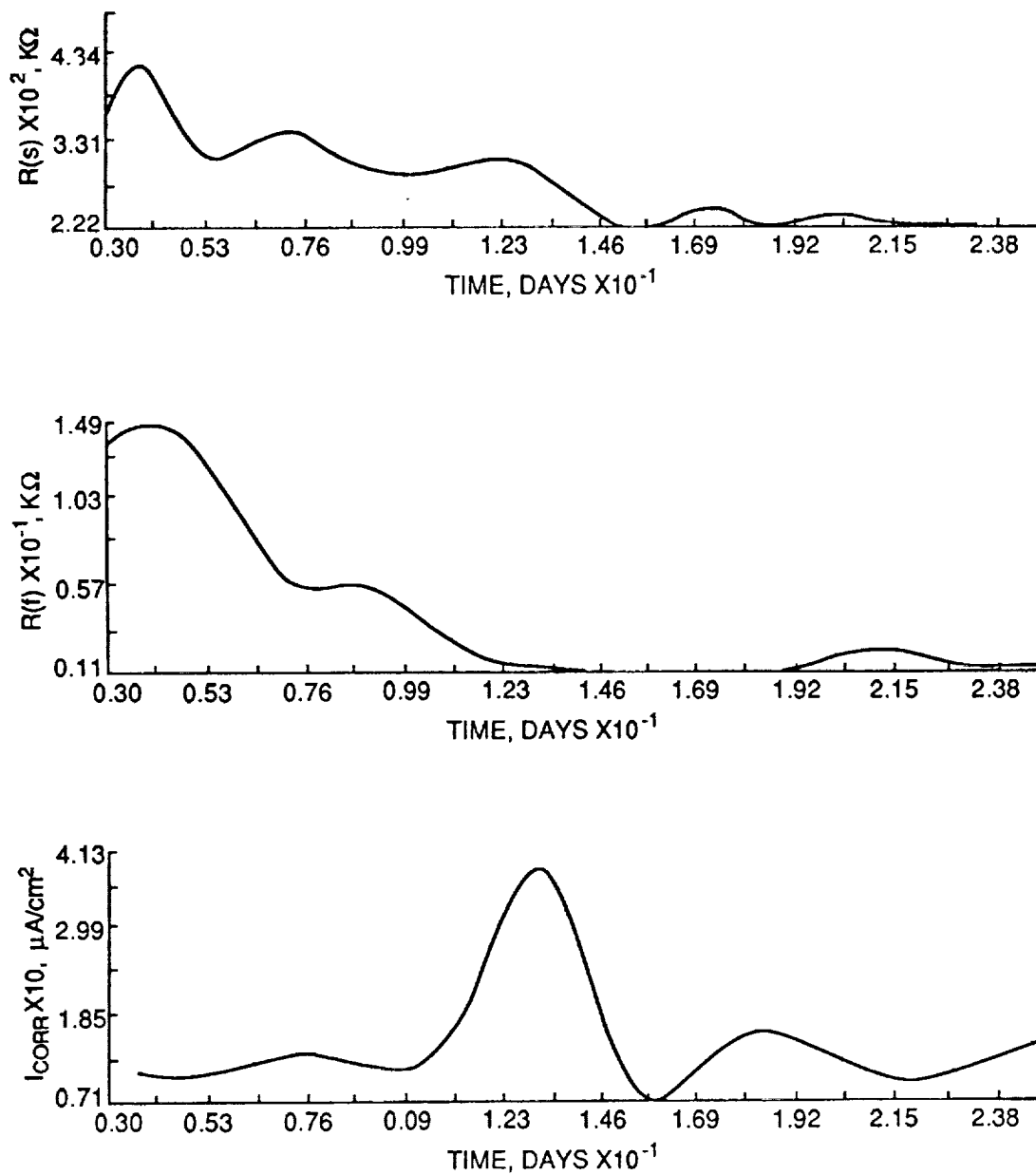


Figure 6.  $R(s)$ ,  $R(f)$ , and  $I_{CORR}$ -time curves for Polylube coat at pH 9.5.



# POLYLUBE, pH 9.5

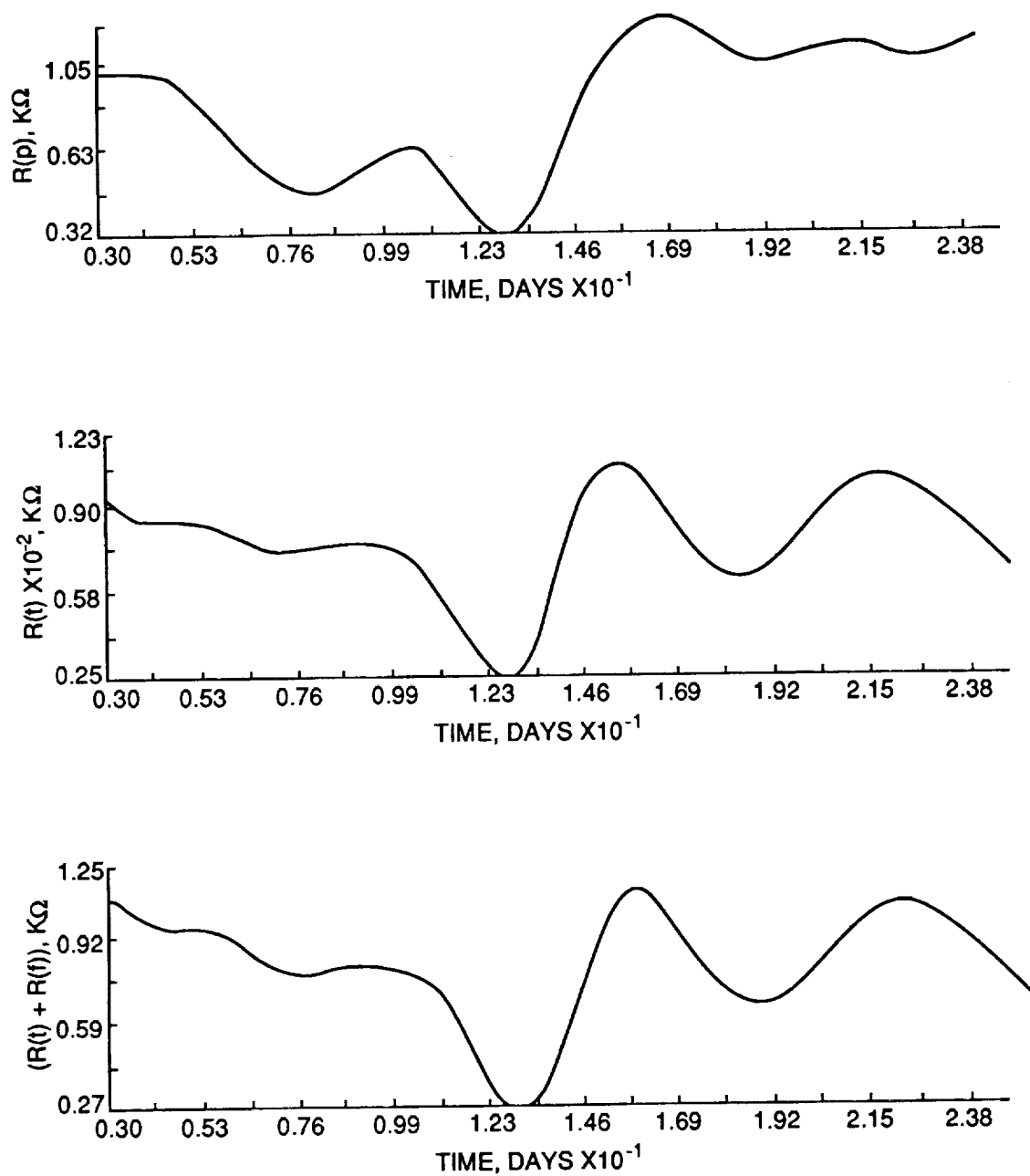


Figure 7.  $R(p)$ ,  $R(t)$ , and  $[R(t) + R(f)]$ -time curves for Polylube coat at pH 9.5.

## POLYLUBE, pH 9.5

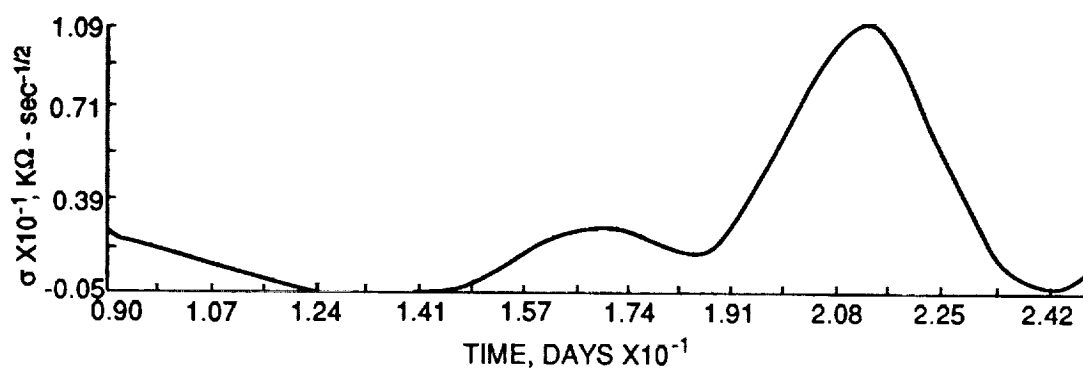


Figure 8. Warburg coefficient-time curve for Polylube coat at pH 9.5.

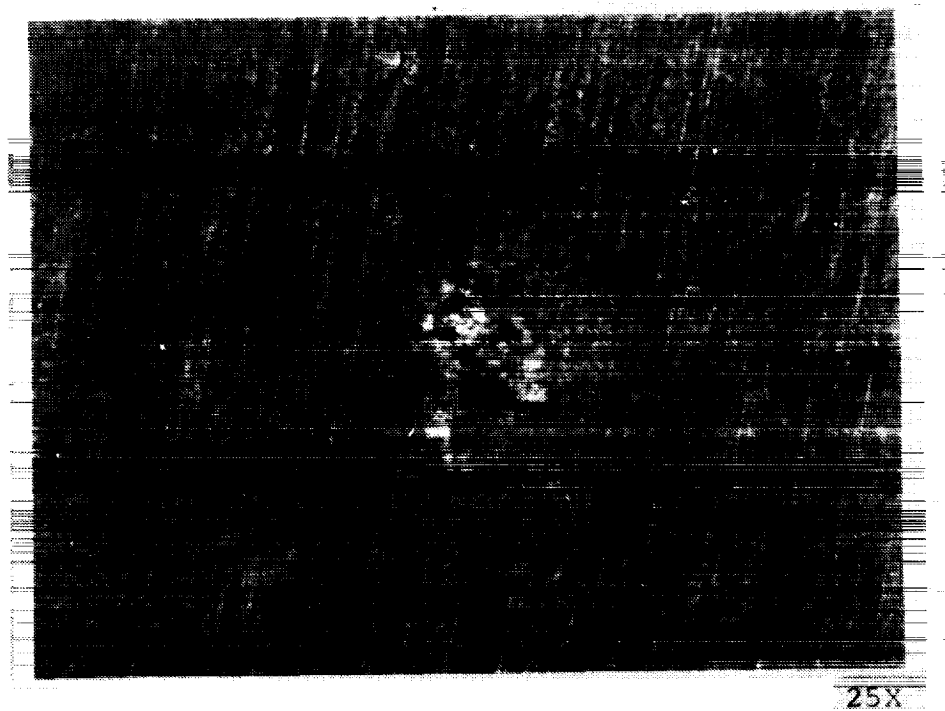


Figure 9. Top view of Polylube sample exposed to 3.5% NaCl solution at pH 9.5 for 28 days.



Figure 10. Cross section of Figure 9 sample showing depth of corrosion pits.

## POLYLUBE, pH 5.5

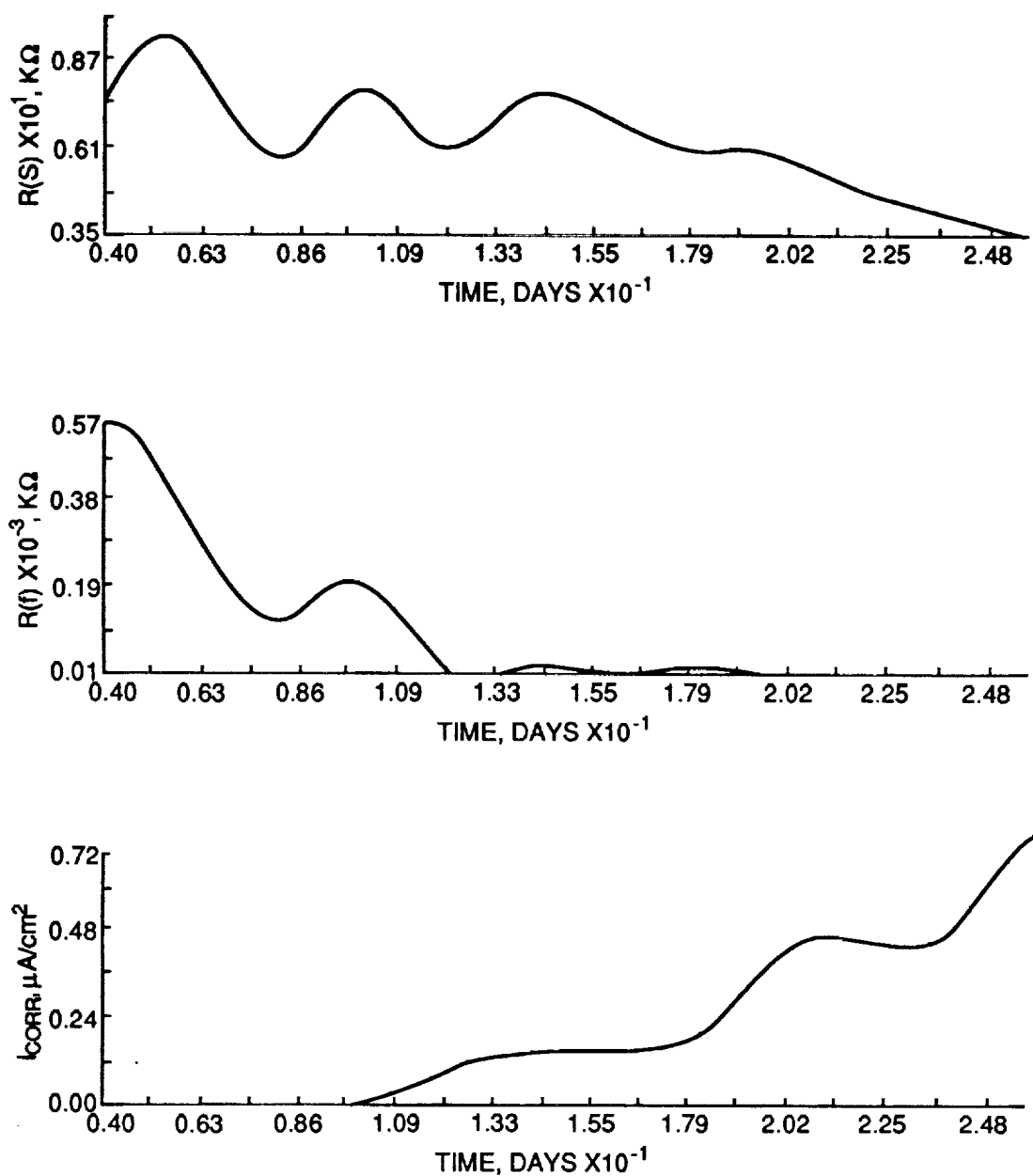


Figure 11.  $R(s)$ ,  $R(f)$ , and  $I_{CORR}$ -time curves for Polylube coat at pH 5.5.

## POLYLUBE, pH 5.5

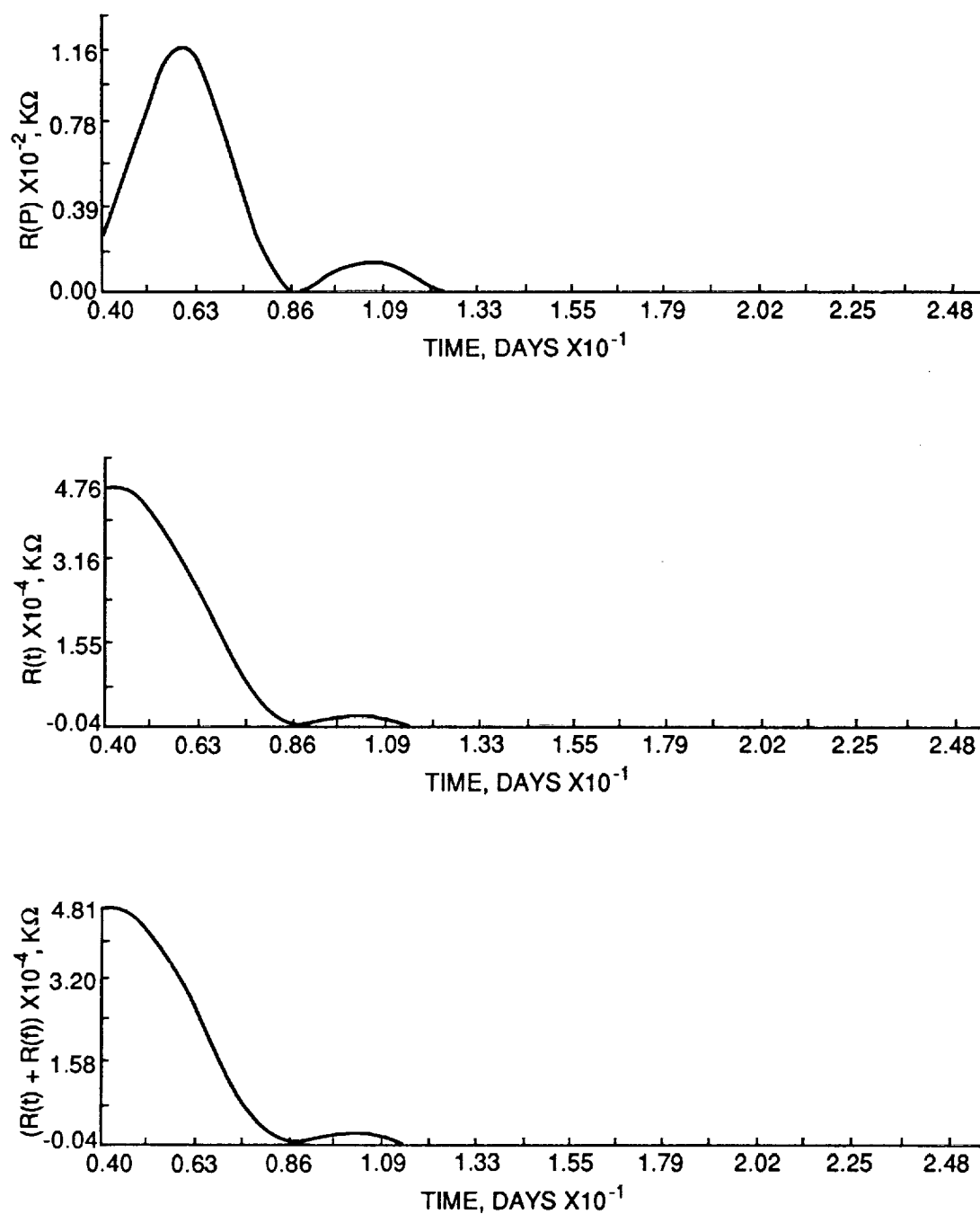


Figure 12.  $R(p)$ ,  $R(t)$ , and  $[R(t) + R(f)]$ -time curves for Polylube coat at pH 5.5.

## POLYLUBE, pH 5.5

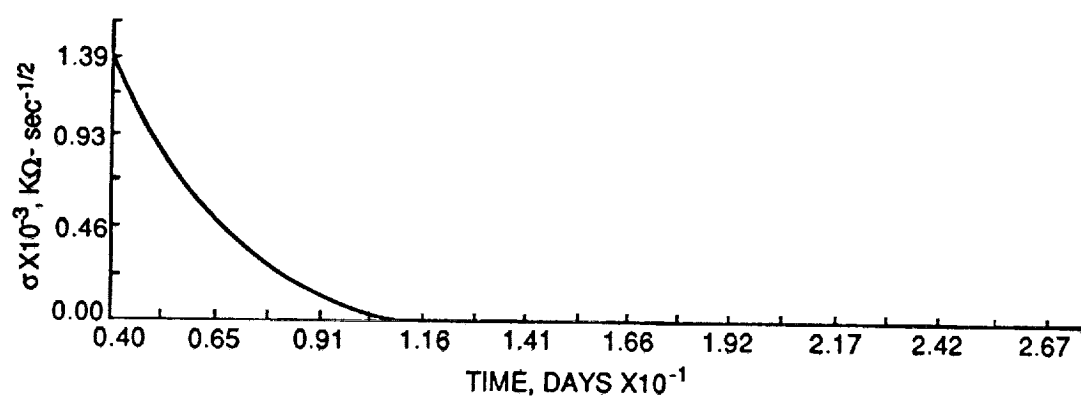


Figure 13. Warburg coefficient-time curve for Polylube coat at pH 5.5.

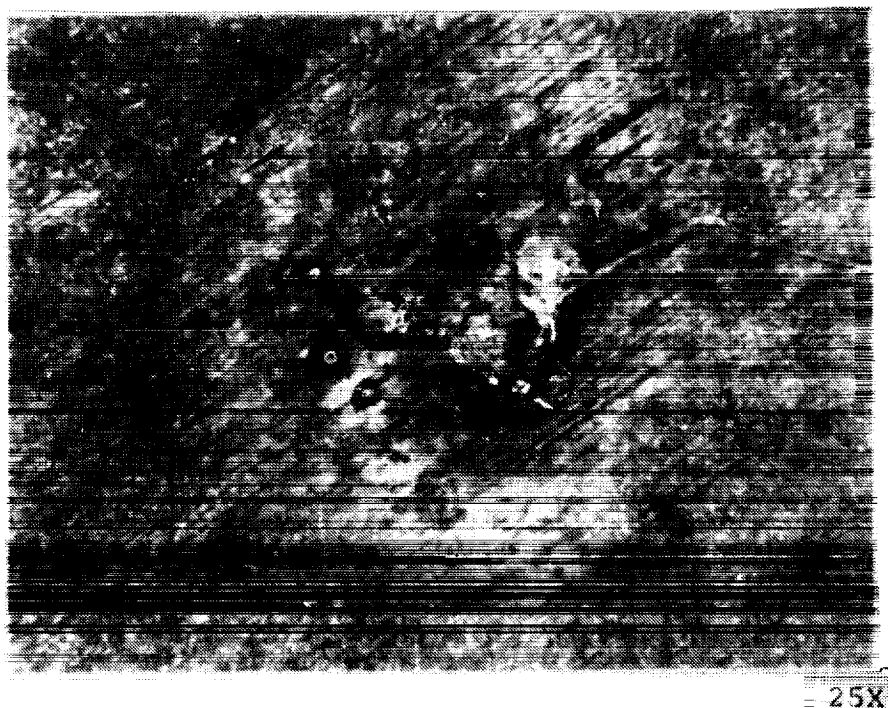


Figure 14. Top view of Polyube sample exposed to 3.5% NaCl solution at pH 5.5 for 28 days.



Figure 15. Cross section of Figure 14 sample showing depth of corrosion pits.

# TUFRAM, pH 9.5

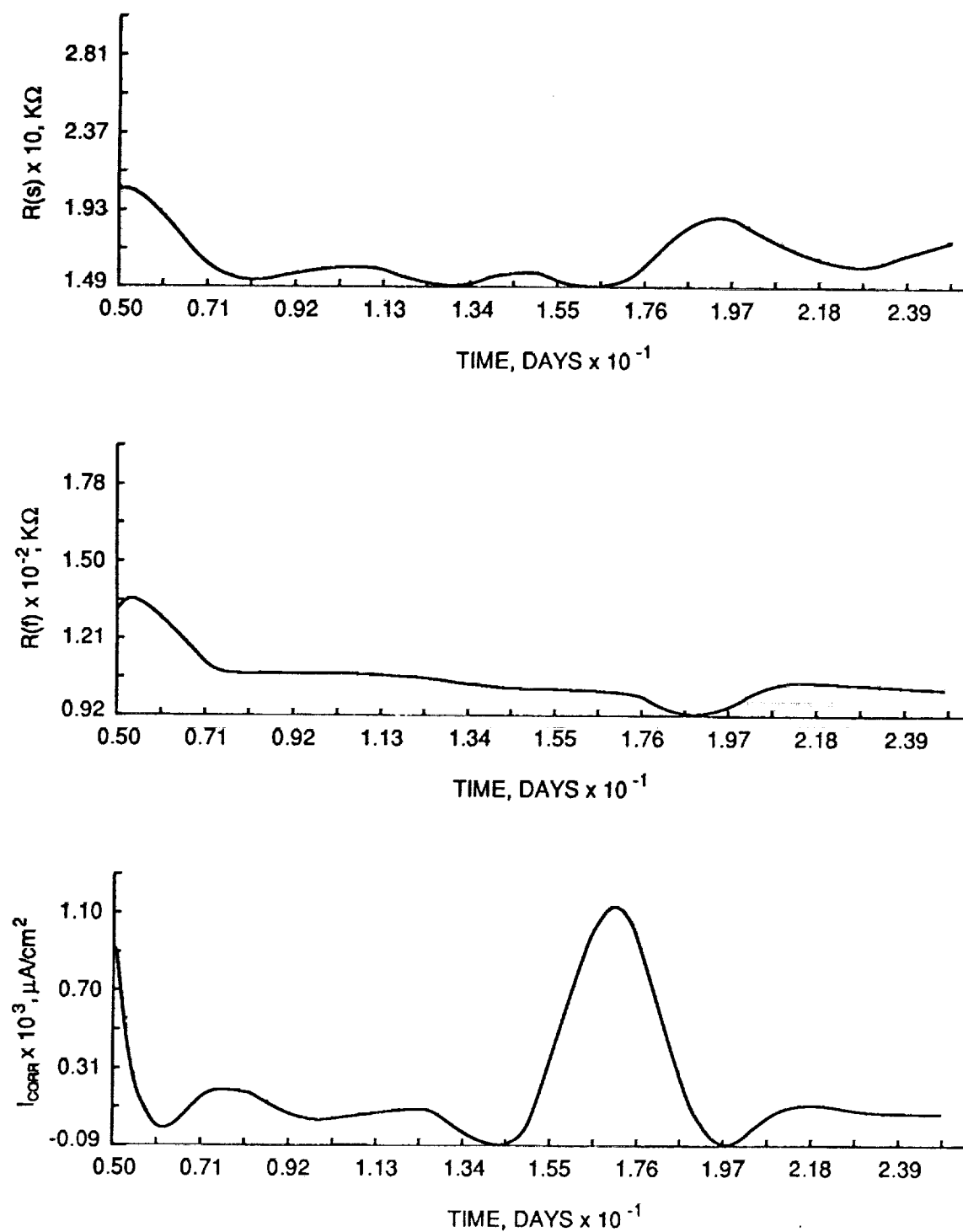


Figure 16.  $R(s)$ ,  $R(f)$ , and  $I_{CORR}$ -time curves for Tufram coat at pH 9.5.



# TUFRAM, pH 9.5

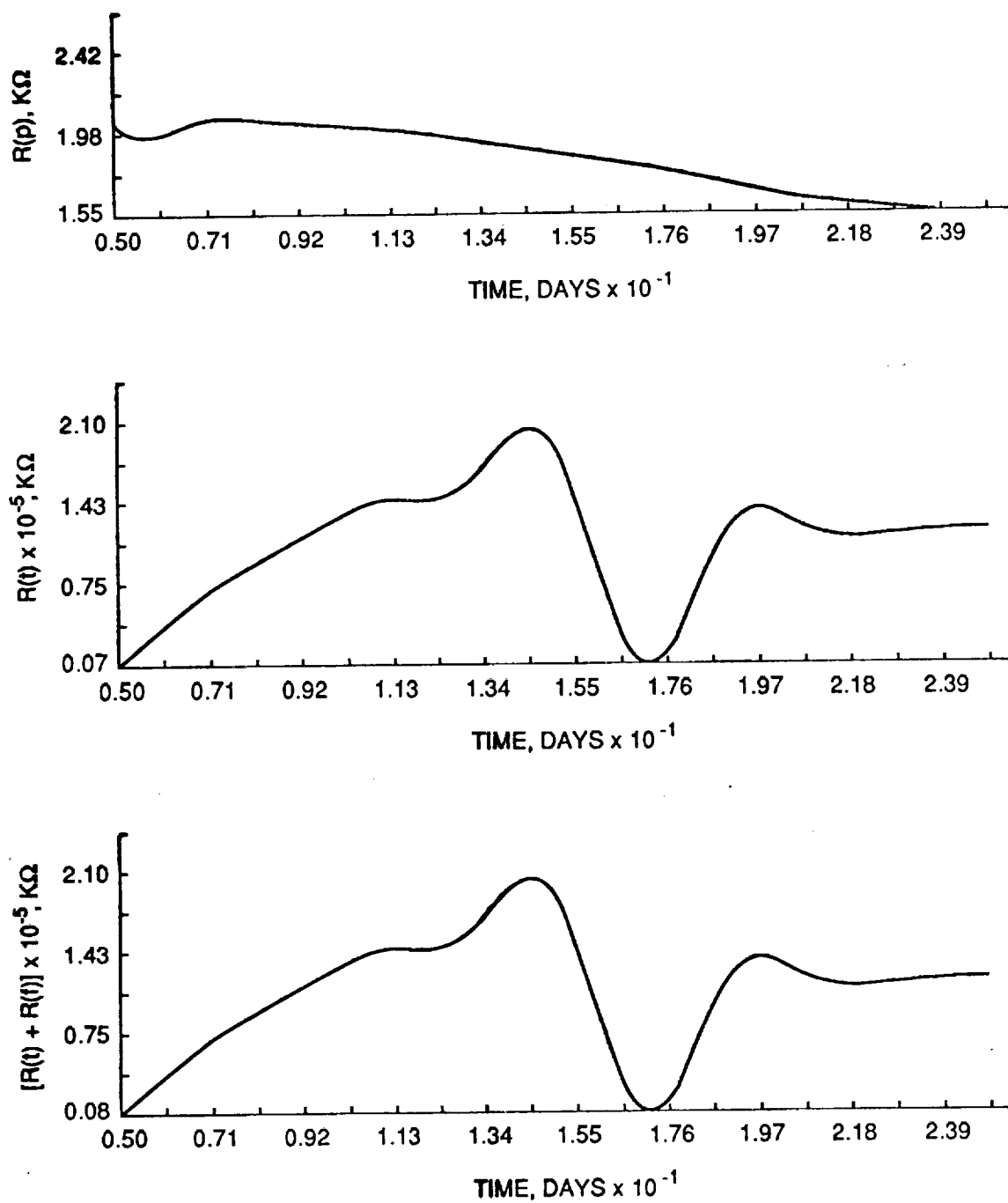


Figure 17.  $R(p)$ ,  $R(t)$ , and  $[R(t) + R(f)]$ -time curves for Tufram coat at pH 9.5.

### TUFRAM, pH 9.5

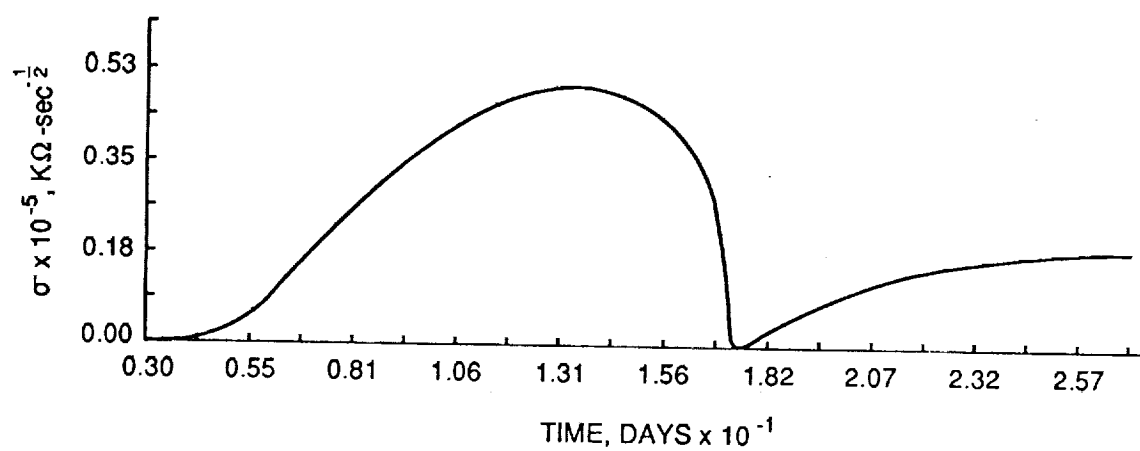


Figure 18. Warburg coefficient-time curve for Tufram coat at pH 9.5.



Figure 19. Top view of Tufram sample exposed to 3.5% NaCl solution at pH 9.5 for 28 days.

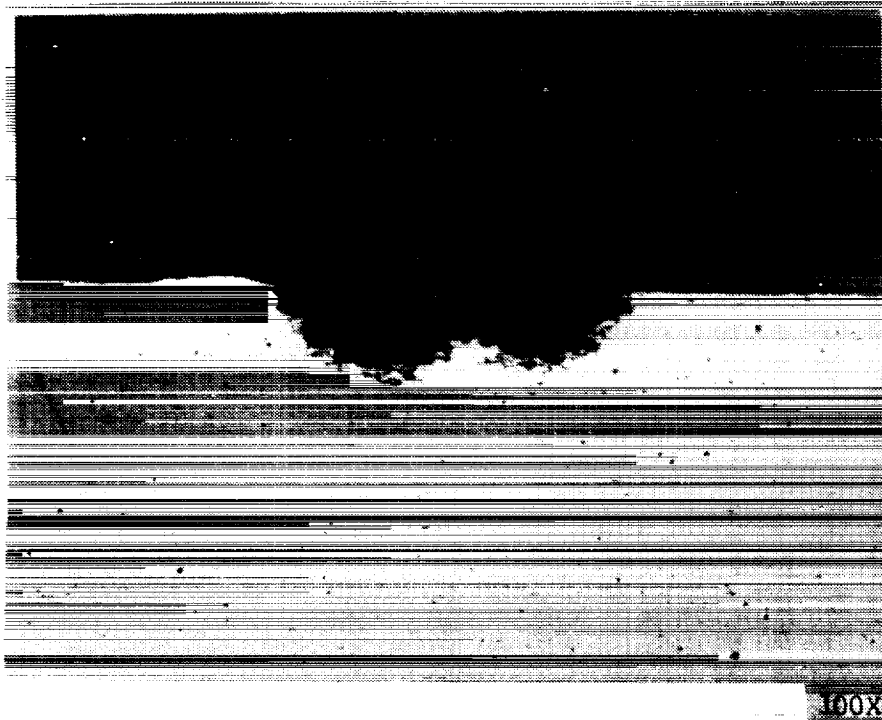


Figure 20. Cross section of Figure 19 sample showing depth of corrosion pits.

# TUFRAM, pH 5.5

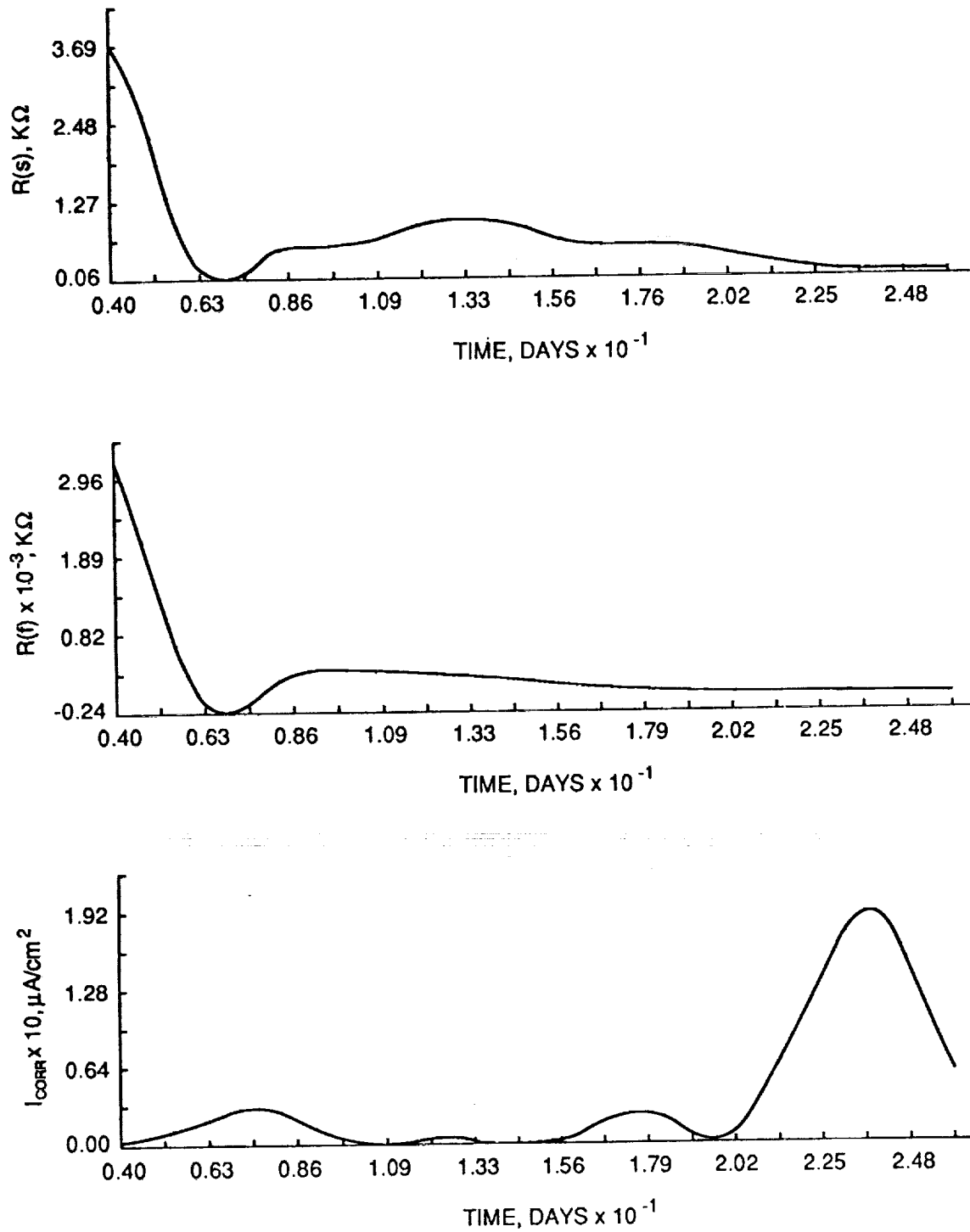


Figure 21.  $R(s)$ ,  $R(f)$ , and  $I_{CORR}$ -time curves for Tufram coat at pH 5.5.

# TUFRAM, pH 5.5

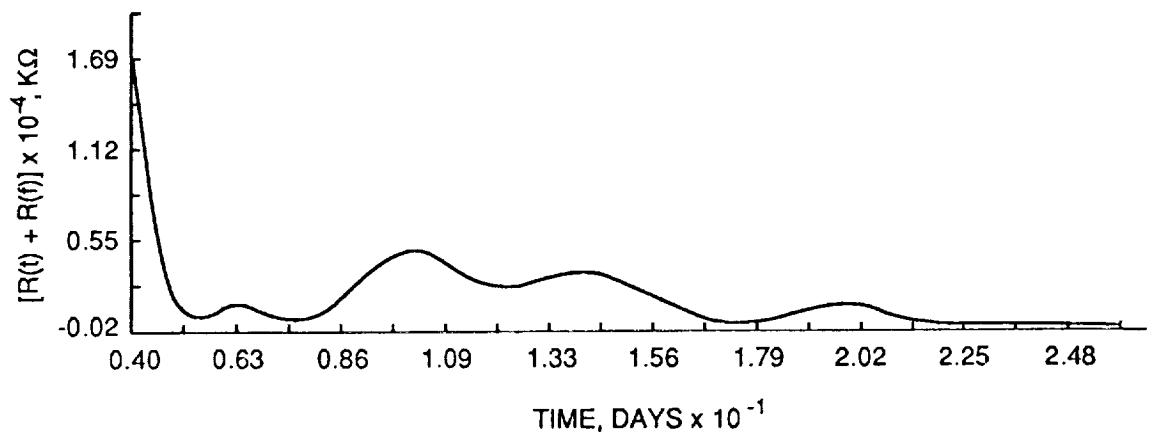
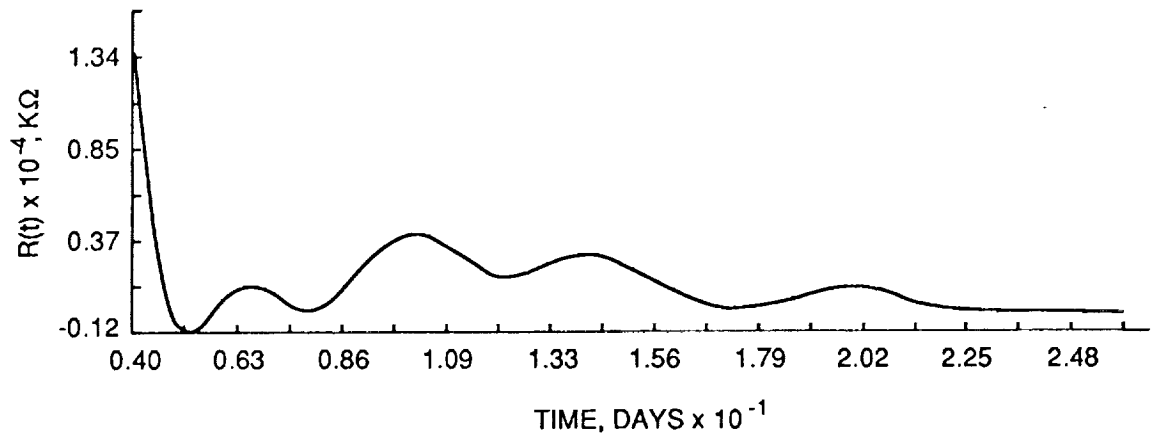
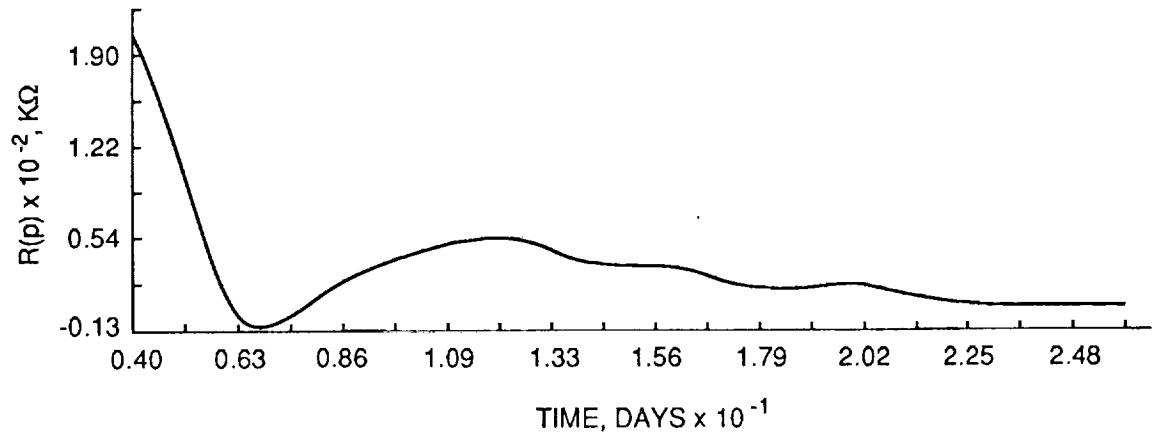


Figure 22.  $R(p)$ ,  $R(t)$ , and  $[R(t) + R(f)]$ -time curves for Tufram coat at pH 5.5.

### TUFRAM, pH 5.5

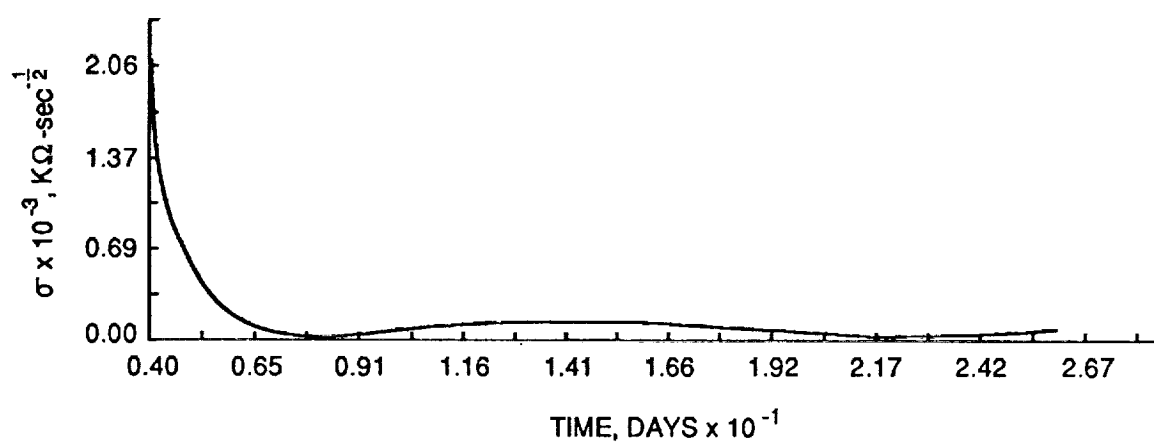
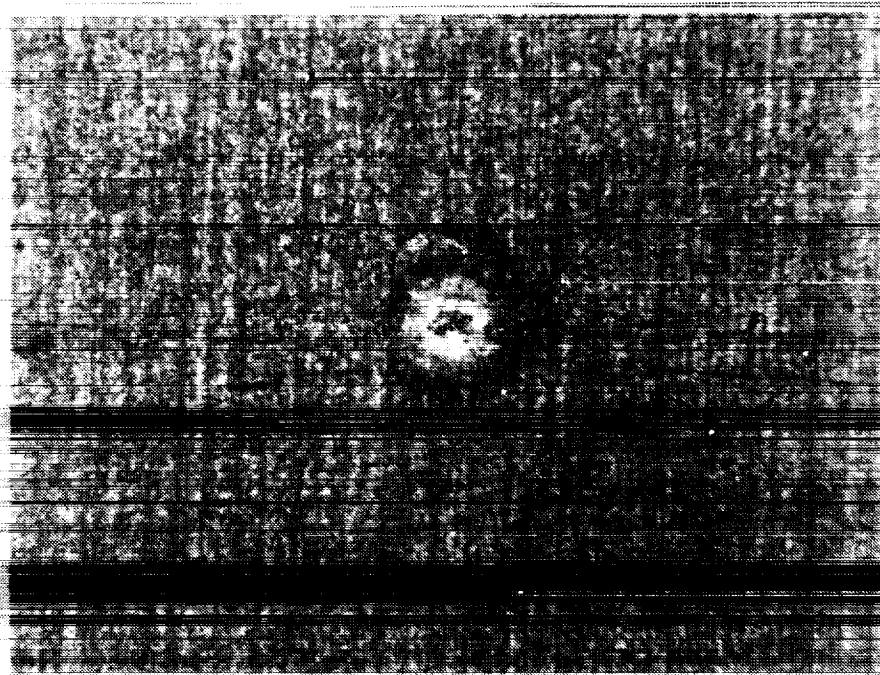
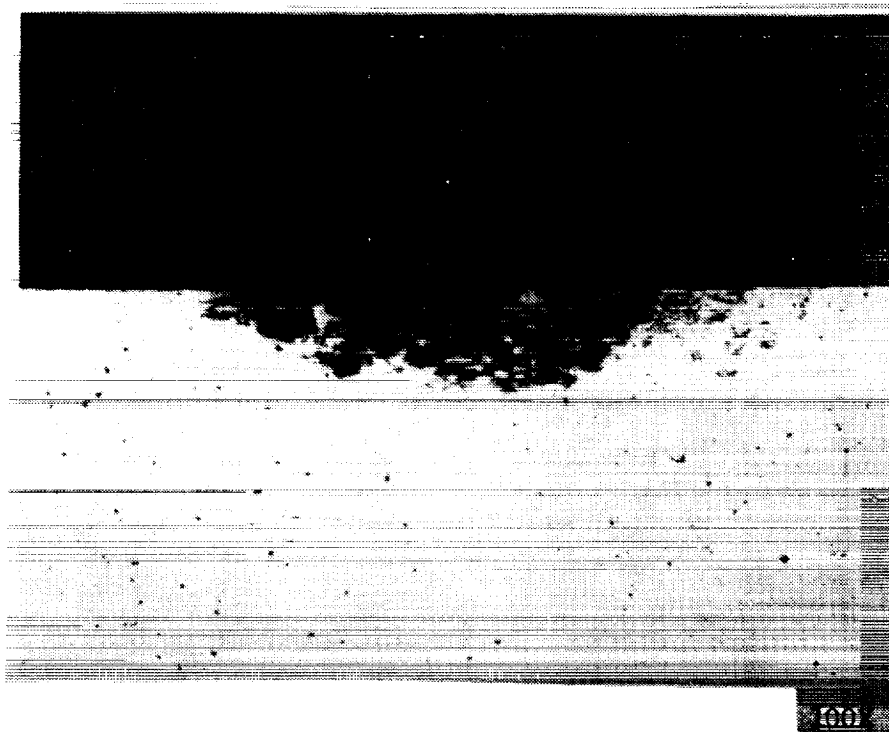


Figure 23. Warburg coefficient-time curve for Tufram coat at pH 5.5.



50X

Figure 24. Top view of Tufram sample exposed to 3.5% NaCl solution at pH 5.5 for 28 days.



60X

Figure 25. Cross section of Figure 24 sample showing depth of corrosion pits.

## HARD ANODIZED, WATER SEALED pH 9.5

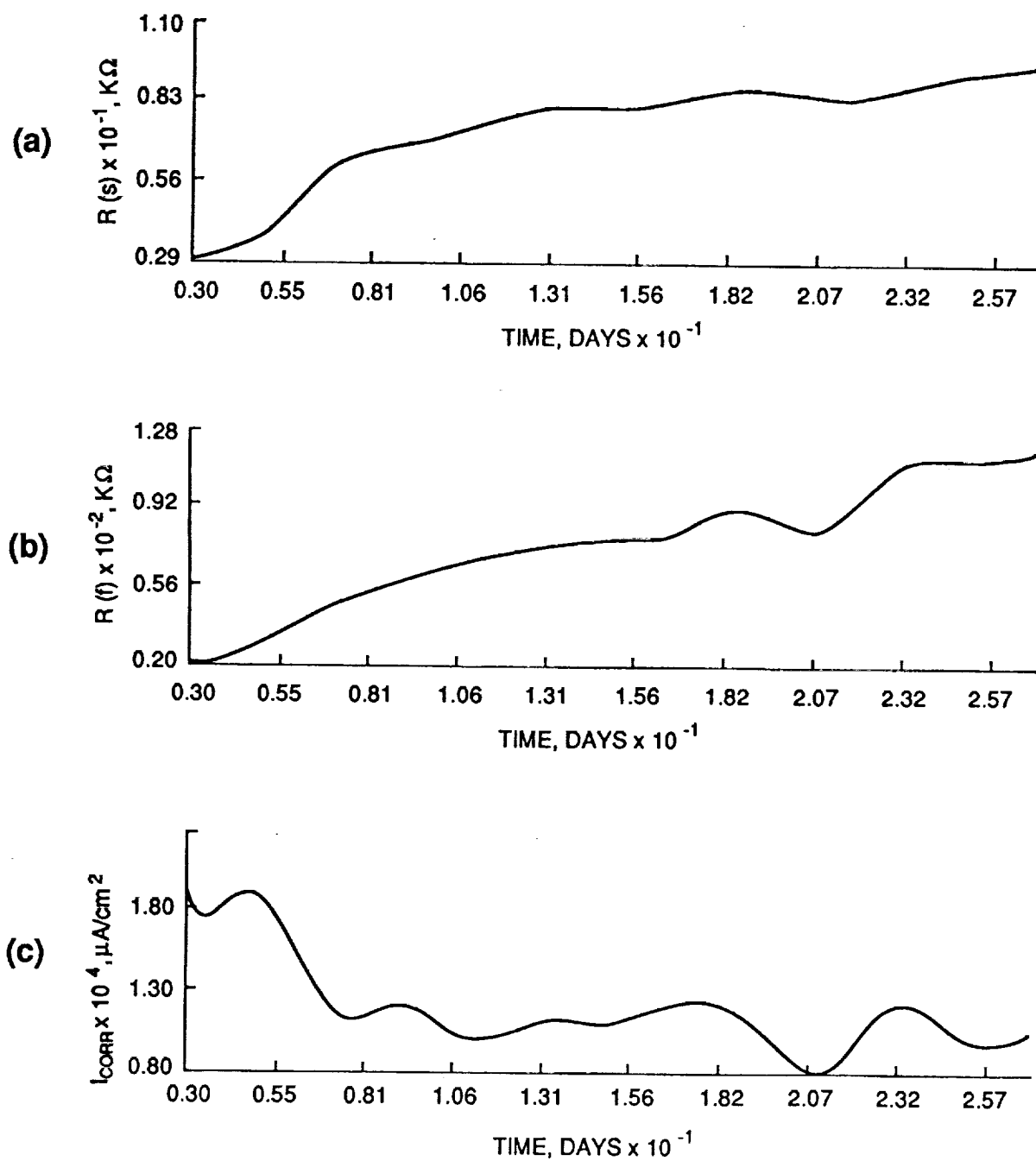


Figure 26.  $R(s)$ ,  $R(f)$ , and  $I_{CORR}$ -time curves for hard-anodized, water-sealed coat at pH 9.5.



# HARD ANODIZED, WATER SEALED pH 9.5

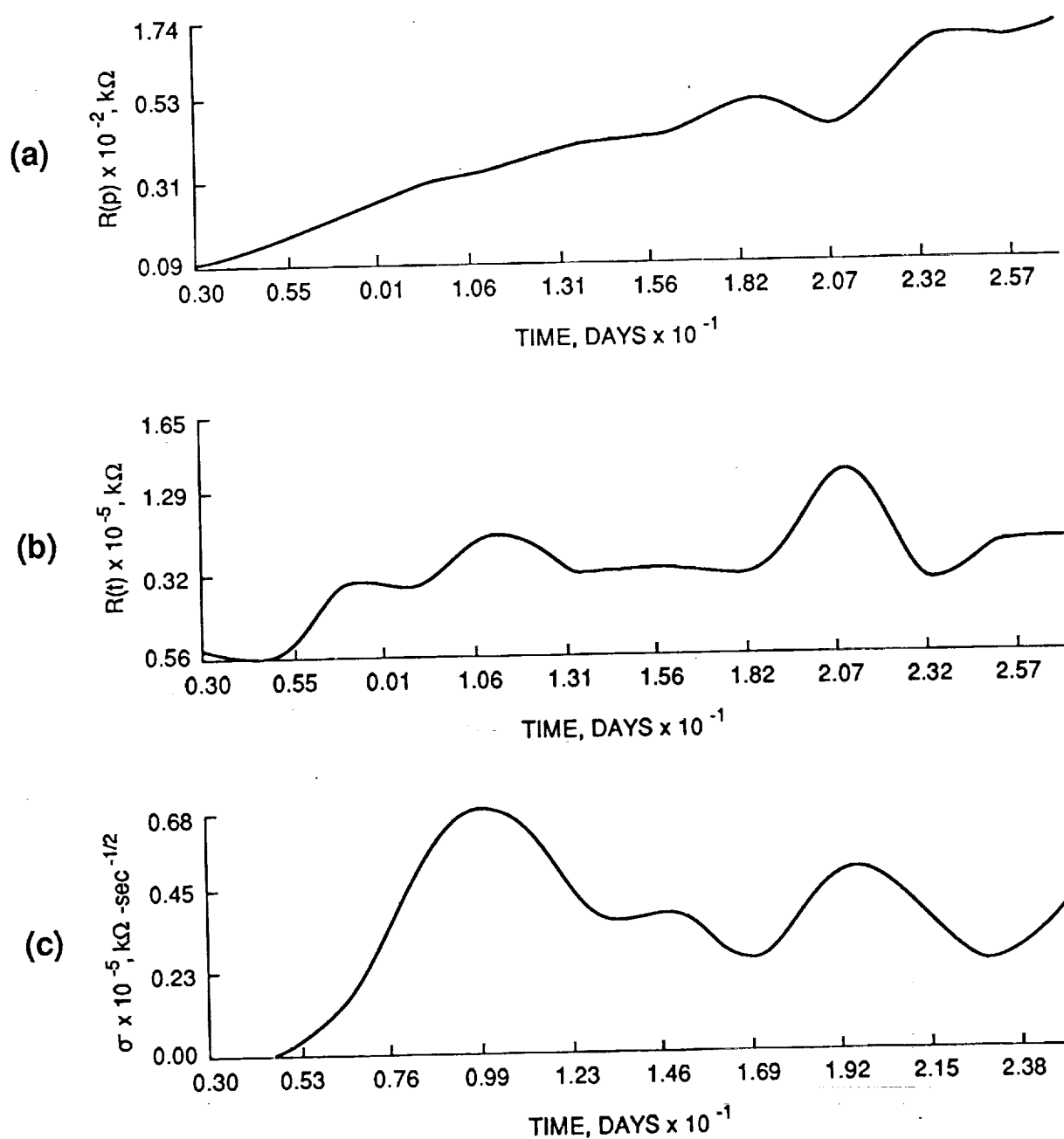


Figure 27.  $R(p)$ ,  $R(t)$ , and Warburg coefficient-time curves for hard-anodized, water-sealed coat at pH 9.5.

## HARD ANODIZED, WATER SEALED pH 5.5

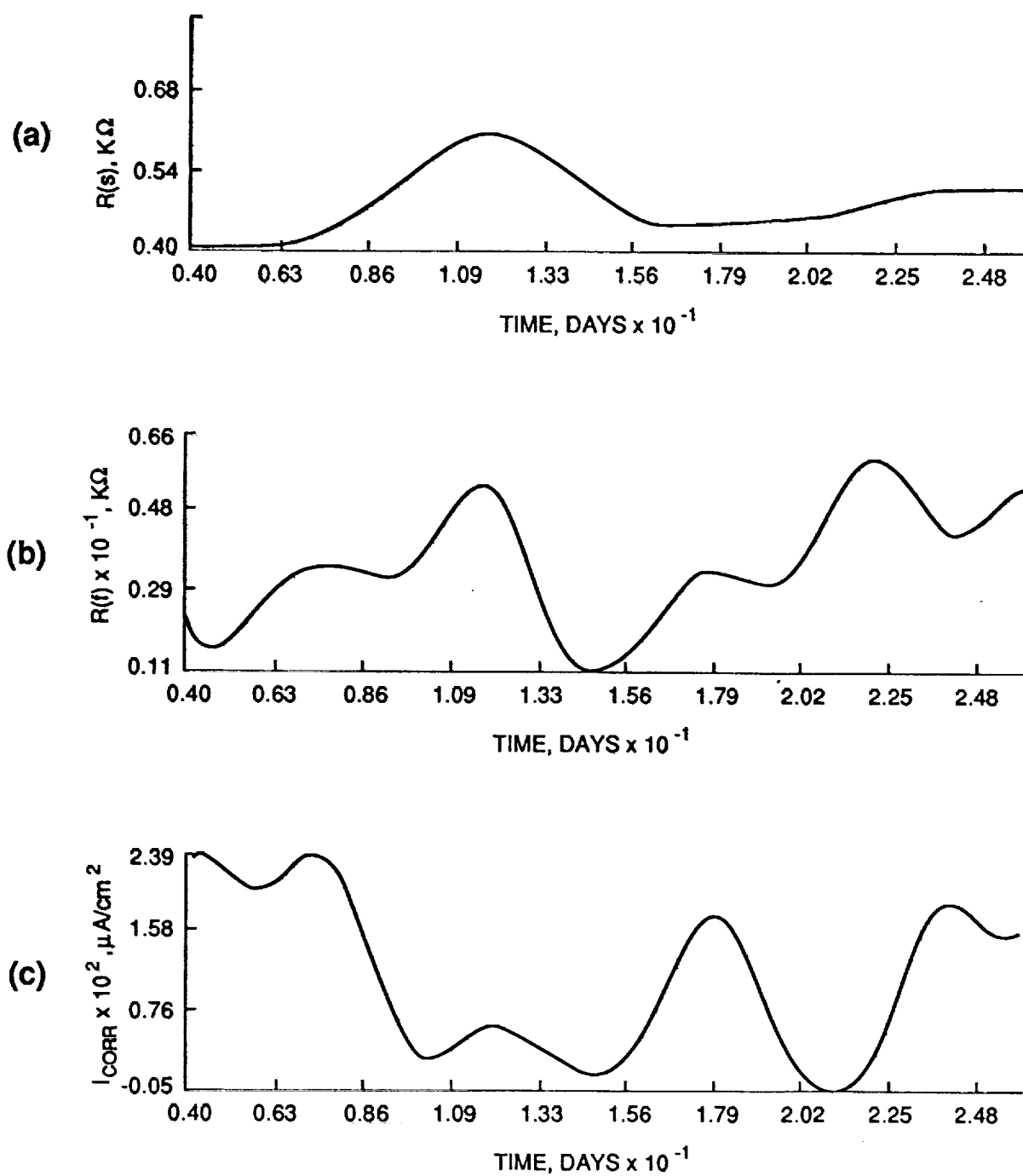


Figure 28.  $R(s)$ ,  $R(f)$ , and  $I_{CORR}$ -time curves for hard-anodized, water-sealed coat at pH 5.5.

# HARD ANODIZED, WATER SEALED pH 5.5

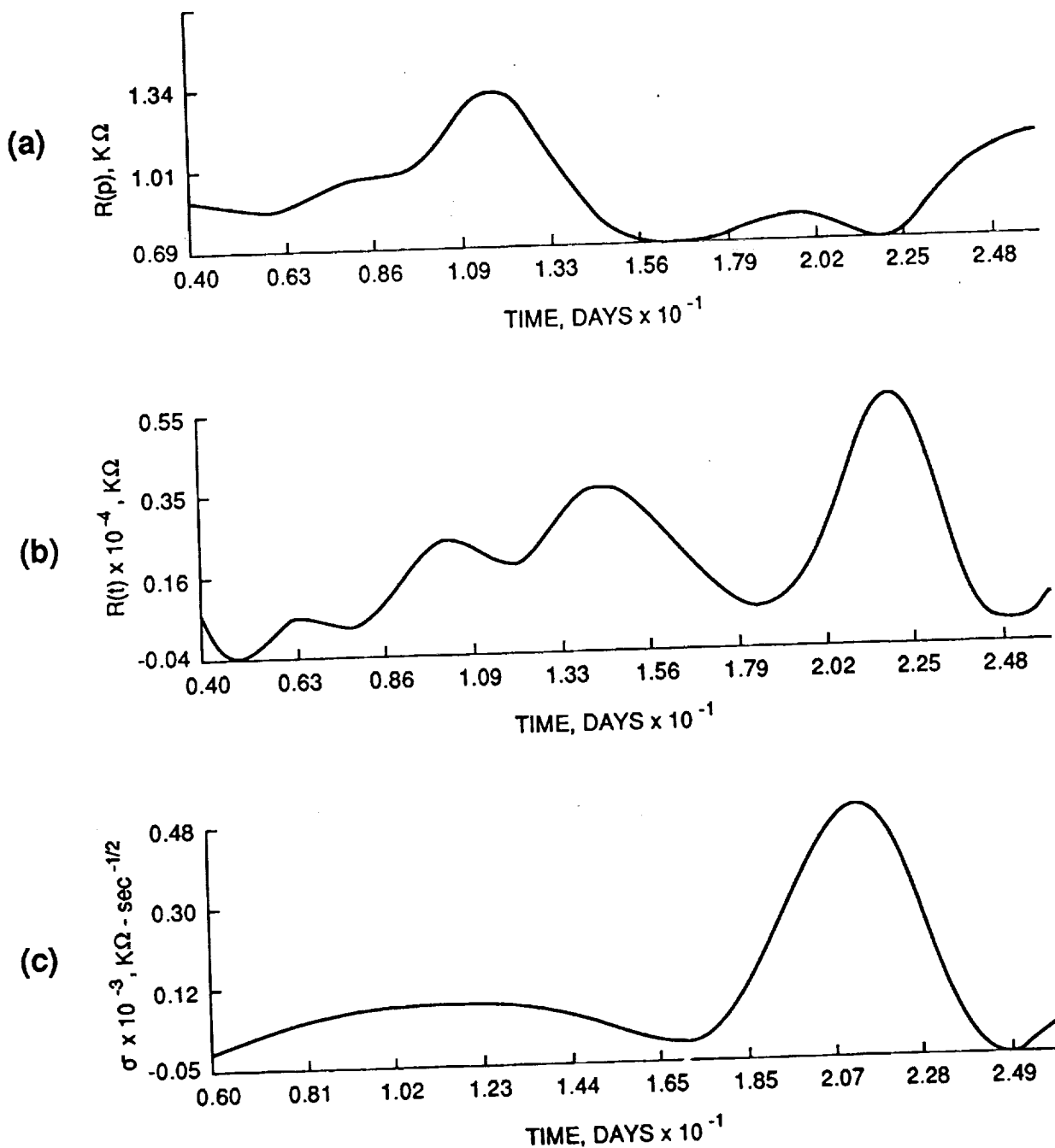
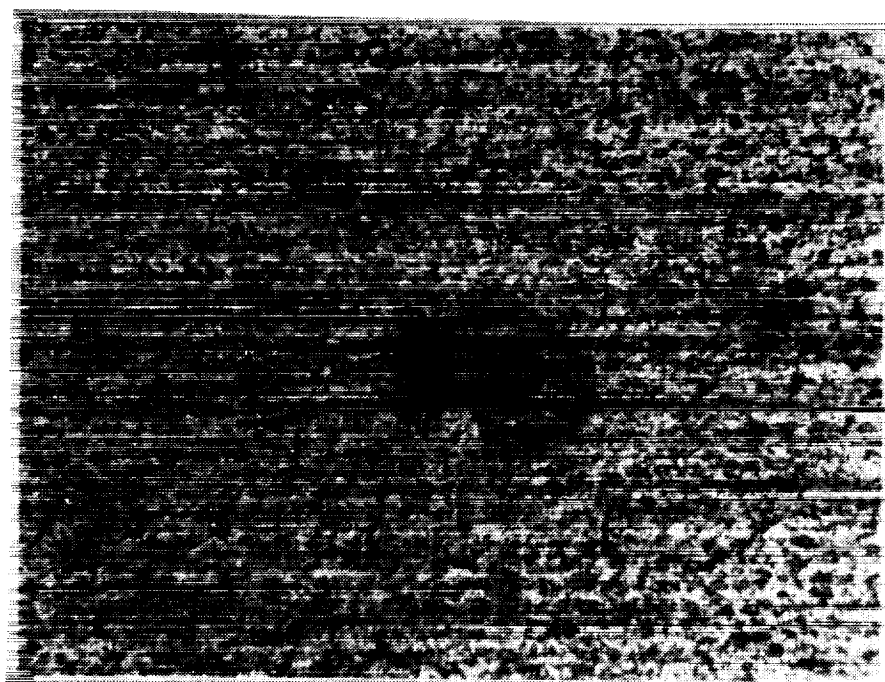


Figure 29.  $R(p)$ ,  $R(t)$ , and Warburg coefficient-time curves for hard-anodized, water-sealed coat at pH 5.5.



31X

Figure 30. Top view of hard-anodized sample exposed to 3.5% NaCl solution at pH 5.5 for 28 days.



50X

Figure 31. Cross sections of Figure 30 sample showing depth of corrosion pit.

# **HARD ANODIZED, DICHROMATE SEALED pH 9.5**

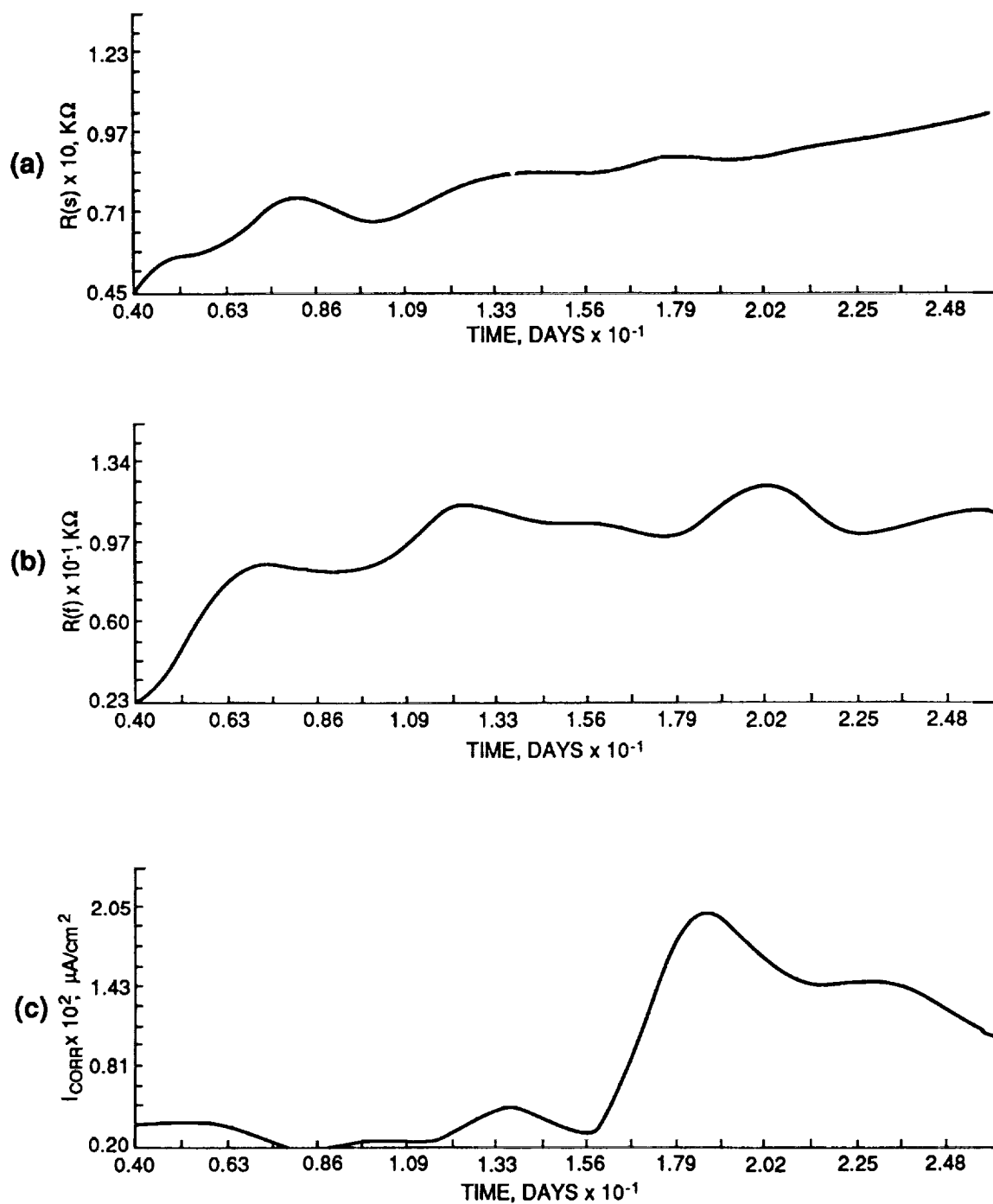


Figure 32.  $R(s)$ ,  $R(f)$ , and  $I_{CORR}$ -time curves for hard-anodized, dichromate-sealed coat at pH 9.5.

# **HARD ANODIZED, DICHROMATE SEALED pH 9.5**

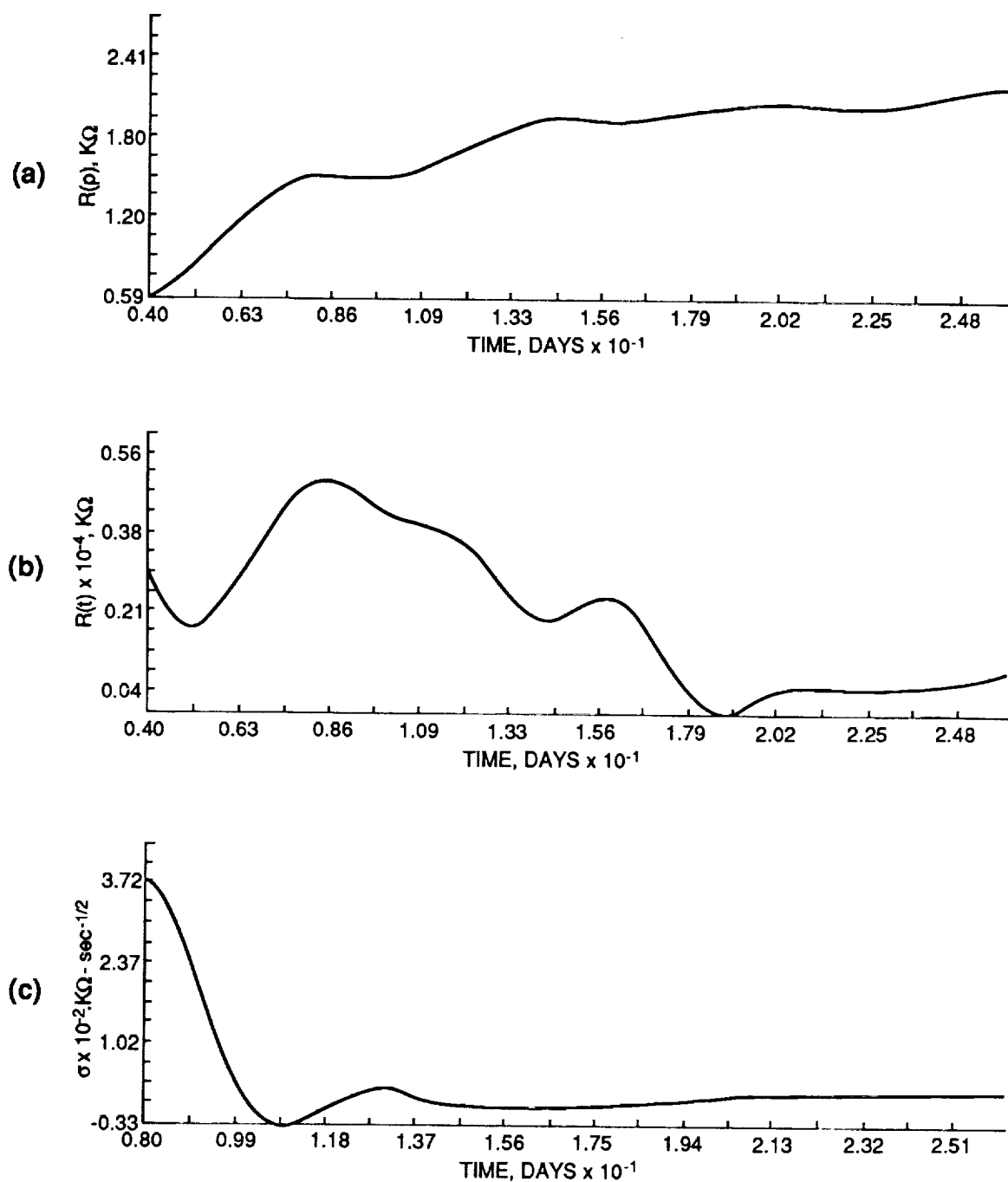


Figure 33.  $R(p)$ ,  $R(t)$ , and Warburg coefficient-time curves for hard-anodized, dichromate-sealed coat at pH 9.5.

# **HARD ANODIZED, DICHROMATE SEALED pH 5.5**

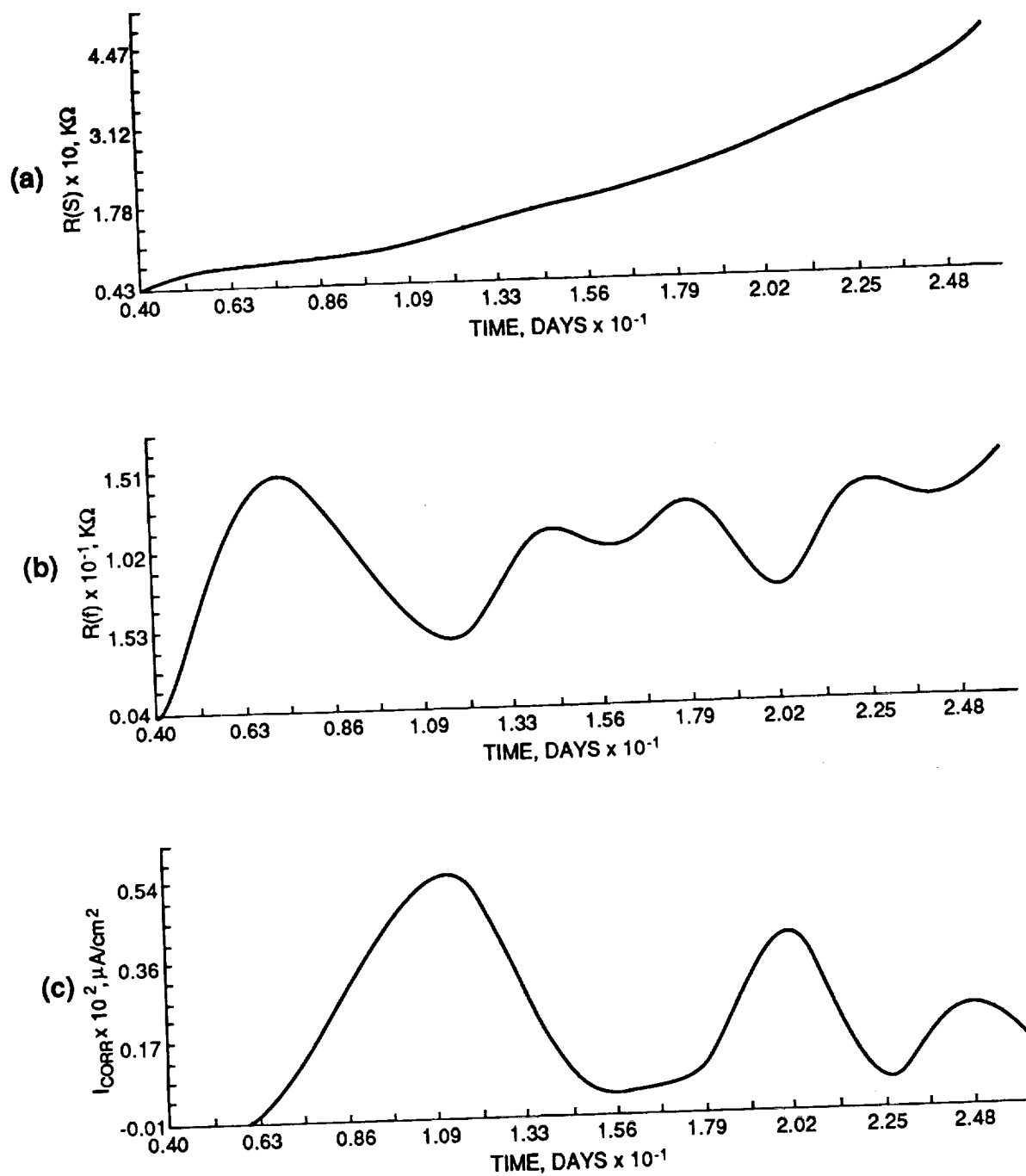


Figure 34.  $R(s)$ ,  $R(f)$ , and  $I_{CORR}$ -time curves for hard-anodized, dichromate-sealed coat at pH 5.5.

# HARD ANODIZED, DICHROMATE SEALED pH 5.5

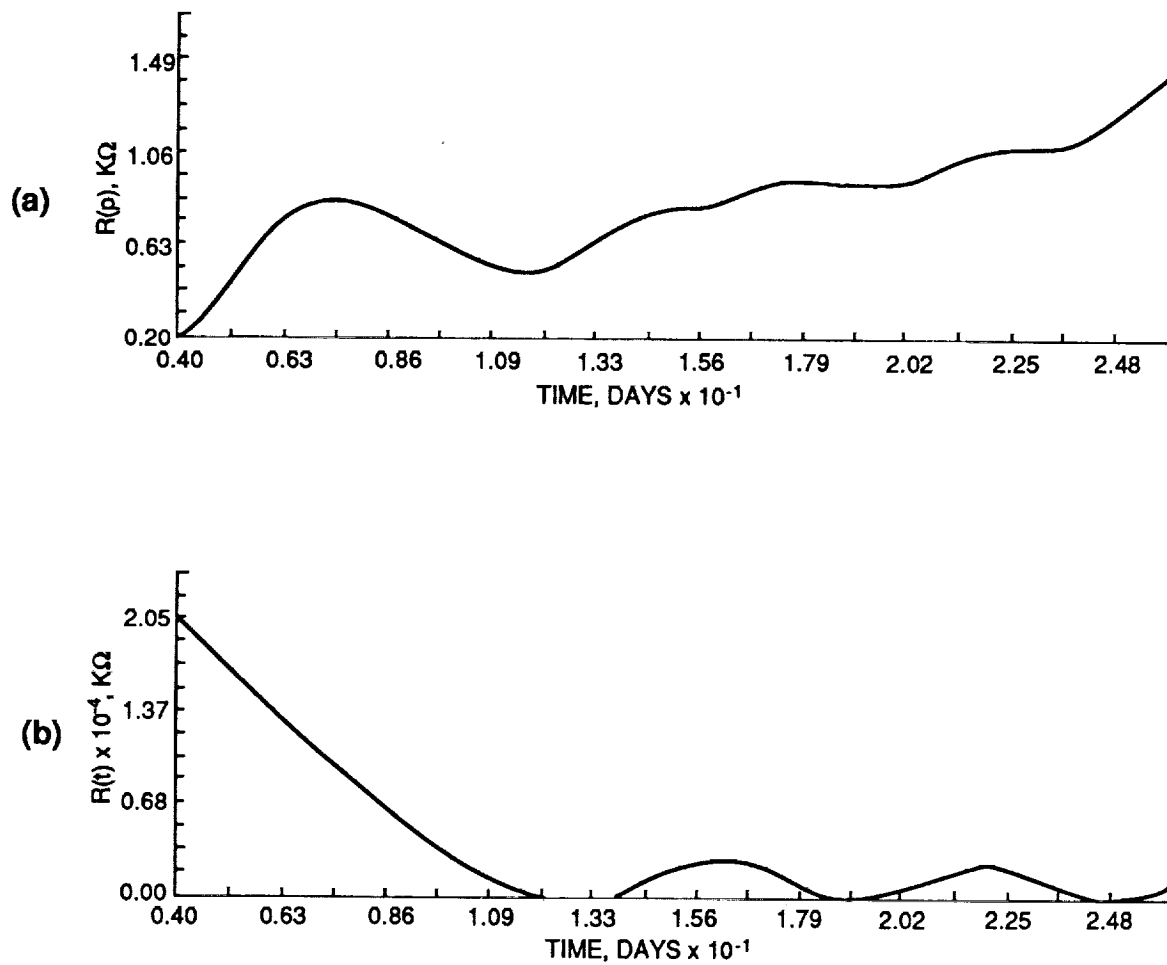


Figure 35.  $R(p)$  and  $R(t)$ -time curves for hard-anodized, dichromate-sealed coat at pH 5.5.



ORIGINAL PAGE  
BLACK AND WHITE PHOTOGRAPH

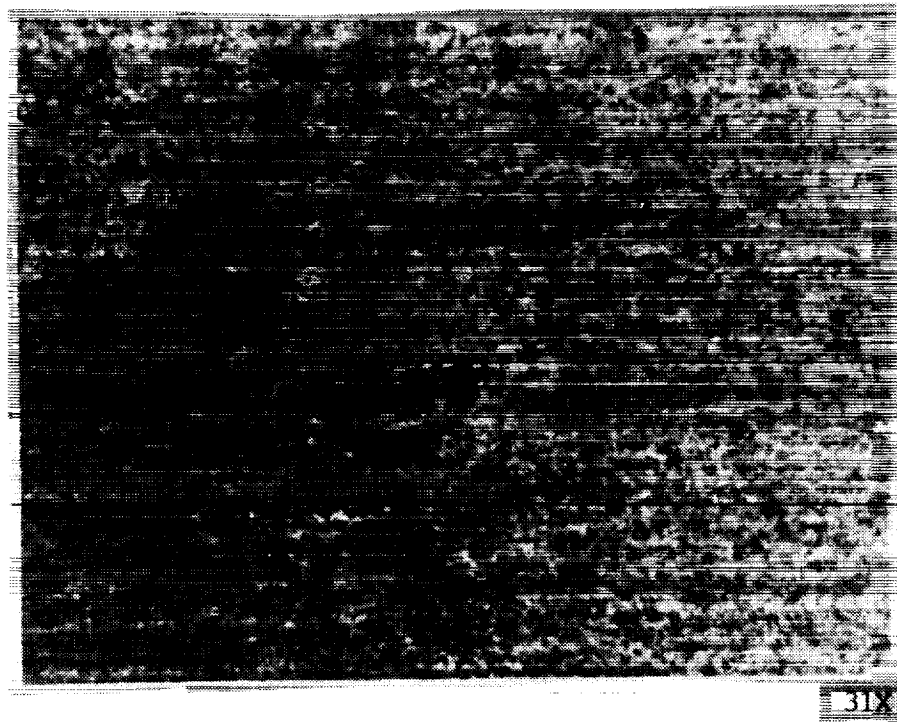


Figure 36. Top view of hard-anodized, dichromate-sealed sample exposed to 3.5% NaCl solution at pH 5.5 for 28 days.

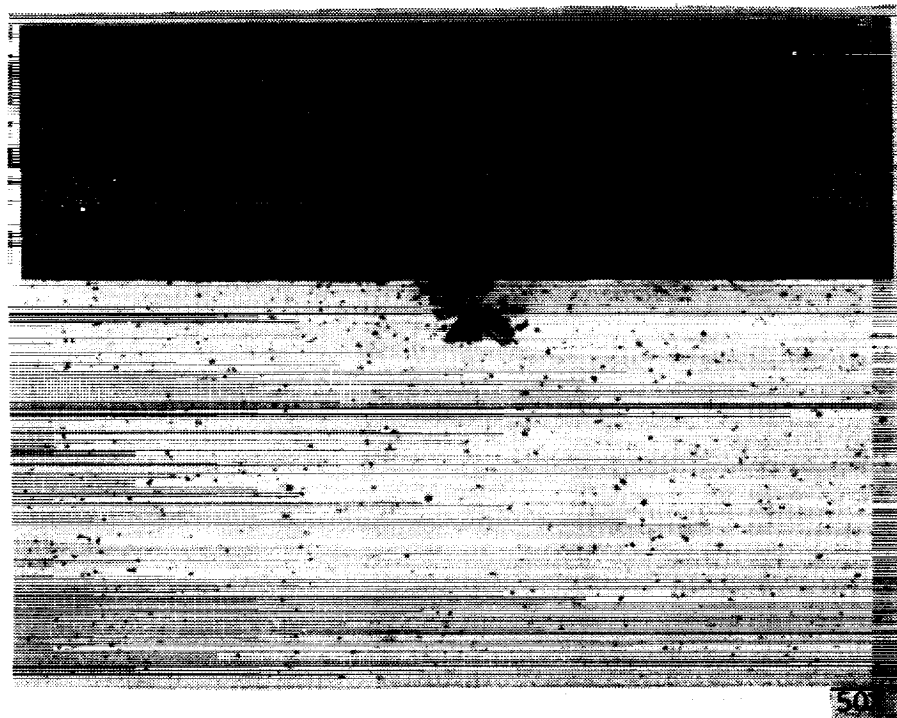


Figure 37. Cross section of Figure 36 sample showing depth of corrosion pit.

## APPROVAL

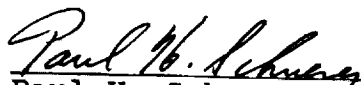
### THE CORROSION PROTECTION OF ALUMINUM BY VARIOUS ANODIZING TREATMENTS

By Merlin D. Danford

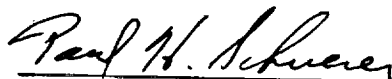
The information in this report has been reviewed for technical content. Review of any information concerning Department of Defense or nuclear energy activities or programs has been made by the MSFC Security Classification Officer. This report, in its entirety, has been determined to be unclassified.



D. B. Franklin  
Chief  
Corrosion Research Branch



Paul H. Schuerer  
Acting Chief  
Metallic Materials Division



R. J. Schwinghamer  
Acting Director  
Materials & Processes Laboratory